remote sensing

Article

Comparison of Bi-Hemispherical and Hemispherical-Conical Configurations for In Situ Measurements of Solar-Induced Chlorophyll Fluorescence

Qian Zhang [1,2,3,†], Xiaokang Zhang [1,2,†], Zhaohui Li [1,2], Yunfei Wu [1,2] and Yongguang Zhang [1,2,4,*]

1 International Institute for Earth System Sciences, Nanjing University, Nanjing 210023, China; zhangqianzh@nju.edu.cn (Q.Z.); dg1827045@smail.nju.edu.cn (X.Z.); mg1727058@smail.nju.edu.cn (Z.L.); DZ1827003@smail.nju.edu.cn (Y.W.)
2 Jiangsu Provincial Key Laboratory of Geographic Information Science and Technology, School of Geographic and Oceanographic Science, Nanjing University, Nanjing 210023, China
3 Collaborative Innovation Center on Forecast and Evaluation of Meteorological Disasters, Jiangsu Key Laboratory of Agricultural Meteorology, Nanjing University of Information Science & Technology, Nanjing 210044, China
4 Collaborative Innovation Center of Novel Software Technology and Industrialization, Nanjing 210023, China
* Correspondence: yongguang_zhang@nju.edu.cn; Tel.: +86-25-8968-1569
† Q.Z. and X.Z. contributed equally to this work.

Received: 24 September 2019; Accepted: 9 November 2019; Published: 12 November 2019

Abstract: During recent decades, solar-induced chlorophyll fluorescence (SIF) has shown to be a good proxy for gross primary production (GPP), promoting the development of ground-based SIF observation systems and supporting a greater understanding of the relationship between SIF and GPP. However, it is unclear whether such SIF-oriented observation systems built from different materials and of different configurations are able to acquire consistent SIF signals from the same target. In this study, we used four different observation systems to measure the same targets together in order to investigate whether SIF from different systems is comparable. Integration time (IT), reflectance, and SIF retrieved from different systems with hemispherical-conical (hemi-con) and bi-hemispherical (bi-hemi) configurations were also evaluated. A newly built prism system (SIFprism, using prism to collect both solar and target radiation) has the shortest IT and highest signal to noise ratio (SNR). Reflectance collected from the different systems showed small differences, and the diurnal patterns of both red and far-red SIF derived from different systems showed a marginal difference when measuring the homogeneous vegetation canopy (grassland). However, when the target is heterogeneous, e.g., the *Epipremnum aureum* canopy, the values and diurnal pattern of far-red SIF derived from systems with a bi-hemi configuration were obviously different with those derived from the system with hemi-con configuration. These results demonstrate that different SIF systems are able to acquire consistent SIF for landscapes with a homogeneous canopy. However, SIF retrieved from bi-hemi and hemi-con configurations may be distinctive when the target is a heterogeneous (or discontinuous) canopy due to the different fields of view and viewing geometries. Our findings suggest that the bi-hemi configuration has an advantage to measure heterogeneous canopies due to the large field of view for upwelling sensors being representative for the footprint of the eddy covariance flux measurements.

Keywords: solar-induced chlorophyll fluorescence; in situ; prism; splitter fiber; hemispherical-conical; bi-hemispherical

1. Introduction

Remote sensing methods have long been used for monitoring vegetation, usually using reflectance-based vegetation indices (VIs) and other vegetation parameters derived from spectral measurements [1]. However, these VIs may fail to detect short-term changes in plant function as most of them do not have a direct connection with the photosynthetic functioning of the plants [2]. Recently, the remote sensing of solar-induced chlorophyll fluorescence (SIF) has become a promising tool to monitor a plant's physiological condition thanks to developments in observational technology during the last decade. Satellite SIF products have been used to estimate regional and global distributions of ecosystem gross primary production (GPP) [3–11].

In support of promoting the application of space-borne SIF in indicating functional parameters and processes, airborne and ground-based image or non-image canopy spectroscopy observations are conducted to investigate the spatiotemporal character of SIF at different observational scales [12–19]. Compared to airborne platforms, either manned or unmanned aircraft, ground-based platforms are easier to operate and can be adapted to various vegetation types. An imaging spectrometer named SPECIM (Spectral Imaging Ltd., Oulu, Finland) has been setup for SIF observation [15]. However, the operation and maintenance of imaging equipment for long-term observations costs too much; therefore, many studies have deployed non-imaging devices. During the past few years, many kinds of instruments were employed for continuous vegetation canopy spectra observation and were usually set up at flux tower sites [20]. Based on prototypes (e.g., TriFLEX, MRI, SFLUOR box, SIF-system) [12,21,22], many improved systems (e.g., FluoSpec, SIFSpec, PhotoSpec) [13,18,23,24] were developed in addition to existing commercial products such as FLoX (JB Hyperspectral Devices UG, Düsseldorf, Germany) and Piccolo Doppio (University of Edinburgh, Edinburgh, UK) [14]. Thus far, the widely accepted spectrometer for SIF measurement is QEPro (Ocean Optics Inc., Dunedin, FL, USA), which has a typical signal to noise ratio (SNR) of 1000 and can be customized with red and far-red regions (mostly 730–780 nm or 650–800 nm) granting the full width half maximum less than 0.3 nm. A spectrometer with full spectral range from 300–1000 nm, such as FLAME, USB2000, HR2000, or HR4000 (all from Ocean Optics Inc.), is often used to measure canopy reflectance, which can be used to calculate typical VIs (e.g., normalized difference vegetation index (NDVI), enhanced vegetation index (EVI)). To collect high-precision data, spectrometers are usually embedded in temperature-controlled box, keeping away from humidity and fluctuation of temperature, which may cause reduces of SNR. Such automatic and long-term mounted systems are able to collect temporally continuous data and to monitor diurnal and seasonal dynamics of SIF, especially to analyze SIF with concurrently measured bioclimatic parameters and carbon flux [18,25–28].

Under natural conditions, the critical process in the measurement of SIF is how to precisely and synchronously measure solar and vegetation radiation as a spectrometer has only one optical path. The ideal case is using two sensors (i.e., two spectrometers for now) to capture the solar spectrum and vegetation spectrum at the same time. However, in practice, the two sensors need highly accurate cross-calibration in order to avoid any spectral shifts and biases created in the data, which is almost impossible for such high spectral resolution spectrometers used for SIF retrieval [29–33]. Therefore, a construction using one spectrometer and with extra protocols enabling a single optical channel to measure both solar and vegetation radiation is recommended. Two general protocols can be considered, namely the single field of view (SFOV), whereby one fiber optic is directly connected to the spectrometer and the fore optic, where light enters the system, rotates upward and downward to collect solar and vegetation irradiance (cosine corrector is mandatory) [17,34] and the duel field of view (DFOV) whereby two fore optics are fixed to measure downwelling and upwelling radiation, respectively, and an extra device (e.g., shutter or prism) is needed to switch between these two paths before light reaches the spectrometer [1,34,35]. Both protocols have their own advantages and disadvantages, e.g., the SFOV one can avoid spectral shift but the mobile joint where the fore optic rotates repeatedly may cause a bending or loss of light and noise to the spectrum, and the DFOV one keeps both two optical paths steady and may be easier to automate without a moving part but hard to avoid light loss and spectral shift in the switching part [1,34,35]. A couple of systems with different constructions are derived from the second protocol [1,13,17,18,20,22,36,37], which is also used in this study. It has the benefit of being adopted with either hemispherical-conical (hemi-con) or bi-hemispherical (bi-hemi) configurations, i.e., whether the upwelling sensor is bare fiber or equipped with a cosine corrector.

Thus far, it seems that the hemi-con configuration was used more in the field than it's counterpart [20,23] although each of them have their own merits. The upwelling sensor of the hemi-con configuration can be installed at the nadir or off-nadir point at any places of interests but is strongly influenced by the sun-target-viewer geometry, which needs to be considered at either a diurnal or seasonal scale [16,38–40]. The bi-hemi configuration collects downwelling and upwelling irradiance in the nadir view direction, having a great advantage of covering a wide area of the target from its almost hemispheric view [17,34] whereas, in contrast, it may also capture non-vegetation signals due to its large view. Another drawback of the bi-hemi configuration is the attenuation of light by the cosine corrector (may up to 70%) that may increase the integration time (IT) of the spectrometer and reduce the SNR.

During the last decade, a variety of observation systems oriented to SIF retrieval were developed and conducted to collect long-term continuous data from different ecosystems. Along with the establishment of SpecNet and EUROSpec, ChinaSpec is also under development [41] but uses different systems from different research groups. To our best knowledge, differences in these existing systems, especially SIF from different systems, have not been specifically investigated yet. In this study, to gather some information about whether SIF from different systems is comparable, we collected four different systems and ran them together with two main aims, namely to compare four systems with different constructions and to compare the two different configurations (hemi-con and bi-hemi) in SIF in situ measurements and their effects on SIF retrievals.

2. Materials and Methods

2.1. Instrumental Constructions

In this study, we chose four observation systems of DFOV protocol for test. Both hemi-con and bi-hemi configurations were also tested. Figure 1A shows the setup of the observation systems. To measure both solar radiation and canopy radiation for SIF retrieval, in most of the SIF observation systems in use, TTL (Ocean Optics Inc., Dunedin, FL, USA), an optical shutter, and splitter fiber are often used to separate the single optical path of the spectrometer into two channels, and to switch between them. Figure 1B shows the schematic diagram of this construction. Three of the four systems used in this study are built from this kind of construction.

We have also developed a new SIF observation system replacing TTL with a device contained a prism for achieving the function of TTL (SIFprism), of which construction is schematically shown in Figure 1C. The main distinction between the two kinds of systems is the different optical path switching methods, which are either TTL with a splitter fiber [18,27] or a prism with a single fiber. The prism is embedded in a box along with an electric motor and is connected to spectrometer by the single fiber optic. The motor controls the directions (right and left) of the prism to receive the downwelling or upwelling radiation, which is then reflected to the output port connected with the spectrometer via the single fiber optic.

SIFprism is controlled by a MATLAB GUI program called NJUspec Controller (Figure A1). NJUspec Controller runs all the tasks of SIFprism, including regulating the temperature of TCB, managing the position of the prism, closing or opening the shutter of the light path, setting the integration time of each spectrum, displaying the running status of the SIFprism system. The collecting processes of spectra through the NJUspec Controller are as follows:

Once the system is started, the NJUspec Controller enables the external TEC of the TCB to ensure the spectrometer is working in a constant 25 °C ambient environment (Figure A2). The internal temperature of the spectrometer is controlled by an internal TEC to ensure that the temperature of charge-coupled device (CCD) is constantly −10 °C (Figure A2). Moreover, temperature and relative humidity sensors are put into the TCB to monitor the environmental dynamic (Figure A2). The temperature and the relative humidity inside and outside of TCB are displayed on the interface (the bottom left in Figure A1) of NJUspec Controller.

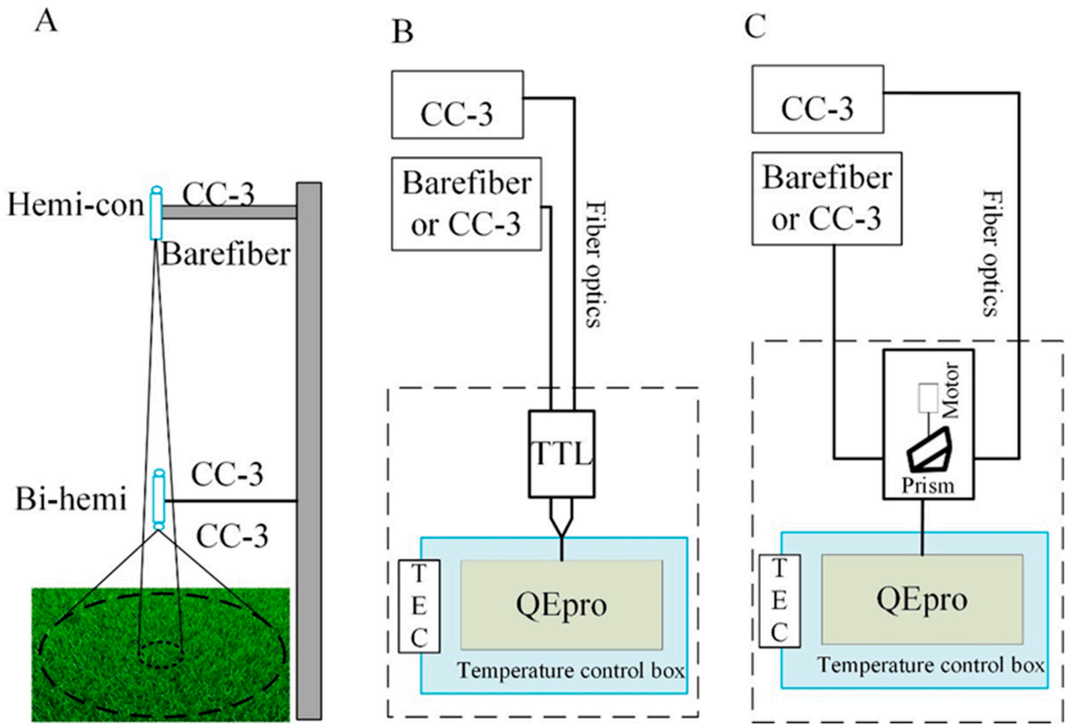

Figure 1. (**A**) Installation diagram of solar-induced chlorophyll fluorescence (SIF) observation systems. The downwelling fiber is equipped with cosine correctors (CC-3; Ocean Optics, Dunedin, FL, USA) and the upwelling fiber is bare, called hemi-con. The downwelling fiber and the upwelling fiber are both equipped with CC-3, called bi-hemi. The downwelling sensor vertically pointed toward the sky to measure bi-hemispheric irradiance and the upwelling was mounted vertically downward to measure the reflected radiance (**B**) Schematic diagram of SIF observation systems equipped with TTL and splitter fiber for switching between two optical paths (irradiance and radiance). Temperature control box (TCB) providing a constant temperature environment, is composed of an external thermoelectric cooler (TEC) and spectrometer (**C**) Schematic diagram of SIF observation systems equipped with prism box.

NJUspec Controller controls the motor to change directions (right and left) of the prism switching between the radiation received from the downwelling and upwelling fiber optics. As data quality is mostly decided by IT, a simple optimal algorithm based on the work of Yang et al. [27] is used to calculate the optimized IT for each spectral measurement to adapt changeable weather conditions. Sequentially, measurements of incident solar radiation, corresponding dark current (DC), reflected canopy radiation and corresponding DC are carried out around every 45 s.

The spectra of radiance and irradiance, and their ITs are displayed on the interface of NJUspec controller (upper-left of Figure A1). The reflectance and both red and far-red SIF of the target are retrieved and also displayed on the interface (upper-right of Figure A1, bottom right of Figure A1), respectively. All these data are saved in a Matlab file (.mat) every 30 min.

In this study, four deliberate observation systems we chose with different constructions (Table 1) to compare SIF retrieved from them. Spectrometers used in all systems were the same model (QEpro) but with different spectral regions and sizes of slit, which were all customized to measure radiance in the fluorescence emission wavelength range. SIF observation system I (SI) and III (SIII) had the same construction, except for the spectral resolution (Full-Width at Half Maximum, FWHM) of the spectrometer (Table 1). Two different optical paths switching methods (Table 1), i.e., TTL and prism, are used in the four systems. SIF observation system II (SII) was the newly built SIFprism. Spectrometers of SI, SII, and SIII were equipped with the same slit (25 µm width), of which the width is much larger than that of the SIF observation system IV (SIV, 5 µm width), which is a widely-used commercial product FLoX (Dual FLuorescence boX; JB Hyperspectral Devices UG, Dusseldorf, Germany).

Table 1. Instrumental constructions of the four SIF observation systems.

Systems	Systems Name	Spectrometer (Spectral Range (nm), FWHM (nm), Slit (µm))	Optical Switching Methods
SI	SIFspec2	QEpro (650–800, 0.3, 25)	TTL and splitter fiber
SII	SIFprism	QEpro (650–800, 0.3, 25)	Prism and single fiber
SIII	Fluospec2	QEpro (730–780, 0.17, 25)	TTL and splitter fiber
SIV	FLoX	QEpro (650–800, 0.3, 5)	TTL and splitter fiber

All systems were radiometrically calibrated using the same and standard procedure in laboratory for several times during the study period to make sure the calibration coefficients could reveal the real-time status of the instruments. Radiometric calibration of the hemispheric fibers CC-3 were performed with a halogen light source (HL-3, Ocean Optics Inc., Dunedin, FL, USA), and the conical bare fibers were done with an integrating sphere (Labsphere, North Sutton, NH, USA).

2.2. Experimental Setup

The experiment was conducted in the Xianlin campus of Nanjing University (32.1147 N, 118.9567 E) of China from May to August 2019. Four observation systems were used to continuously collect spectra of vegetation, soil, and standard reference of grey panel (Labsphere, North Sutton, NH, USA). *Epipremnum aureum* (*E. aureum*, the right in Figure 2) has a small leaf inclination angle which can reduce the influence of canopy structure and was planted in a plastic flowerpot. In total, thirty flowerpots with little difference in terms of growth status were used in this study. In order to reduce the impact of the background, a black cloth was laid beneath all the flowerpots (the left in Figure 2). *E. aureums* were placed outside for 3 weeks before the experiment to adapt to the high light conditions. In addition, dry soil and grey reference with reflectance around 0.5 were chosen as the observation targets to evaluate the stability of the four systems. In this study, two different installation configurations, i.e., hemi-con (the upper in Figure 1A) and bi-hemi (the lower in Figure 1A) were employed to do four tests (Figure 3) as shown below.

Test 1: Inter-comparison of the four systems of hemi-con configuration.

The configuration of hemi-con was adopted for all four observation systems (the upper in Figure 1A) to compare the consistency and difference among the four systems. The downwelling fibers (Figure 2A) pointed toward the sky were bundled together and the height between the fibers and the ground was 1.8 m. The upwelling fibers (Figure 2B) with nadir view were bundled together to measure *E. aureums* canopy, soil surface, and grey panel. The heights between the upwelling fibers and the three targets were 2.6 m (1.15 m diameter FOV), 2.9 m (1.29 m diameter FOV), and 15 cm (6.65 cm diameter FOV), respectively. Figure 4 showed the experiment setup and the bare fiber with 25 degrees field of view (FOV) downward pointing to the vegetation. During the experiment, the measurement of *E. aureums* canopy and soil was conducted from 07:00 to 18:00 local time, and the measurement of grey panel was from 10:00 to 14:00 local time. IT, reflectance, and retrieved SIF from the four systems will be analyzed to evaluate the performance of them when measuring different targets under different conditions.

Test 2: Comparison of bi-hemi and hemi-con configurations with similar field of view (FOV).

Different from Test 1, the configuration of bi-hemi was adopted in SI, SII and SIII, while their downwelling fibers were the same as Test 1 to compare the difference between hemi-con and bi-hemi configurations. The heights between the fibers and *E. aureums* canopy and soil surface were 0.7 m and

1 m, respectively. The hemi-con configuration of SIV remained unchanged and treated as a reference for comparison, the measurements of which proved to be reliable. The heights between the upwelling fiber of SIV and *E. aureums* canopy and soil surface were still 2.6 m and 2.9 m, respectively. The lower heights of SI, SII and SIII were set to restrict the FOV of their upwelling sensors mainly covering the vegetation canopy. The measurement of *E. aureums* canopy and soil was conducted from 07:00 to 18:00 local time.

Figure 2. Experimental setup (**left**) and the conical footprint (**right**) of the four systems. (A) in the left shows the position of downwelling sensor and (B) shows that of upwelling sensor. The red ring in the right represents the field of view (FOV) of the conical upwelling sensor.

Test 3: Comparison of bi-hemi and hemi-con configurations with same upwelling view heights.

Test 2 tested the configurations of bi-hemi and hemi-con at different heights. Considering SIF retrieved from sensors at different heights may be affected by different viewing and atmospheric conditions, the only difference in here Test 3 from Test 2 was that the same height between the upwelling fibers of four observation systems and *E. aureums* canopy were 0.7 m, and the observation target was only *E. aureums* to directly compare the difference between conical and hemispheric upwelling sensor.

Test 4: Comparison of bi-hemi and hemi-con configurations over homogeneous canopy.

Grass canopy is more homogeneous than the *E. aureums* canopy and is continuous, reducing the effects of canopy heterogeneity and interference from background. Therefore, we designed Test 4 for a comparison of SIF retrieved from bi-hemi and hemi-con configurations between these two different canopies. The direct aim of this test is to find out if the results of bi-hemi and hemi-con configurations could be the same as the results of the two configurations in Tests 2 and 3, which were quite different. The configurations of bi-hemi and hemi-con were only adopted in SII and SIV (Figure 4), respectively. Their upwelling fibers were mounted at the same height (0.5 m) above the canopy of relatively homogeneous grass to measure reflected spectra. Furthermore, the upwelling fiber of SII and the upwelling fiber of SIV were then mounted 0.5 m and 1 m above the canopy to test if different heights of the upwelling sensors affect the results, respectively.

Finally, we compared the performance of the four observation systems and the two different configurations (hemi-con and bi-hemi) according to integration time (IT), reflectance, and SIF from them, respectively (the orange ellipse in Figure 3).

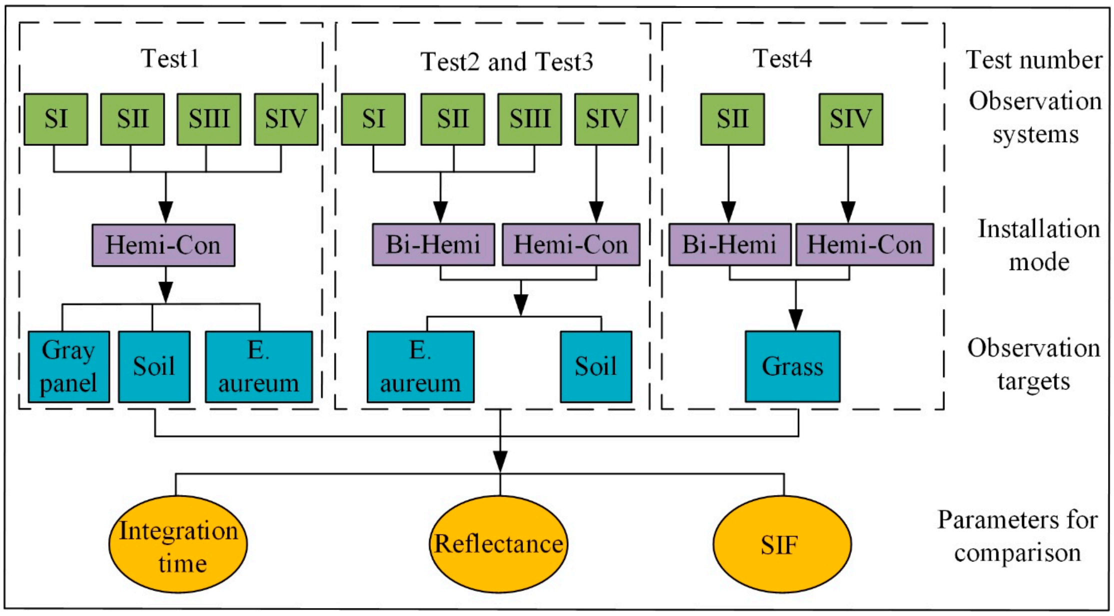

Figure 3. The scheme of the tests. Green boxes are four observation systems (SI, SII SIII and SIV); purple boxes represent the different configurations of observation systems in each test; blue boxes are observation targets including grey panel, soil and *E. aureum*; orange ellipse are the variables used for the comparison of four observation systems.

Figure 4. The configurations of bi-hemi with larger footprint (blue circle) and hemi-con with small footprint (red circle) with systems II and IV (SII and SIV) at a homogenous grassland field.

2.3. A Test for the FOV of CC-3

Conceptually, a cosine corrector can collect incident light from 180° FOV [42]. However, Liu et al. [43] simulated the FOV of CC-3 and indicated that about 90% radiation captured by CC-3 was supplied by 140° FOV. Therefore, we designed a test to measure the "true" FOV of CC-3 (Figure 5). First, a piece of 5 m^2 black cloth was laid on the ground to shield the signal of the ground. Second, we selected two pots of *E. aureums* with good growth status put on a removable pallet. Third, the configuration of bi-hemi was adopted in SII, and the upwelling fiber was mounted at 1 m height from *E. aureums* canopy. Finally, we moved the pallet from the center of CC-3 FOV under the upwelling fiber every 0.2 m from the origin to 3 m. The experiment was conducted around noon local time and finished within half an hour to make sure it was done under stable and constant illumination.

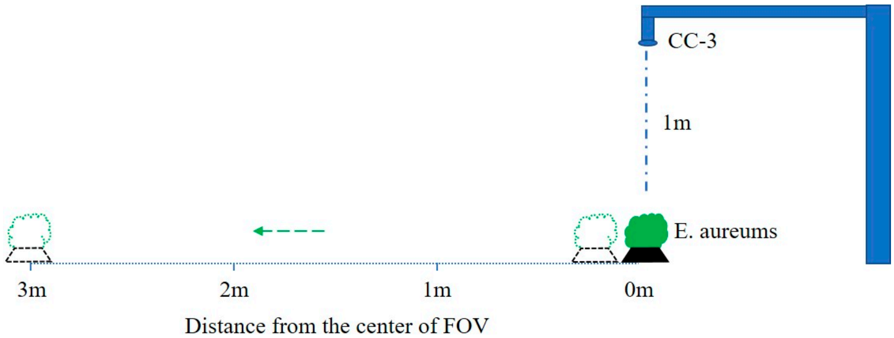

Figure 5. Diagram of measuring the field of view (FOV) of cosine corrector (CC-3).

2.4. SIF Retrievals

Algorithms based on the Fraunhofer line depth (FLD) principle [44,45] are most commonly used for SIF retrievals at the canopy level. The FLD method needs spectral measurements at two channels, one inside and one outside a Fraunhofer line [46]. It assumes that reflectance (r) and SIF are constant at the two channels. However, in fact, these two variables have significant differences at the two channels, especially for r at 687 nm and SIF at 760 nm [37,47]. One of the FLD-based algorithms, the three-band FLD (3FLD) method, has been proposed and proved to be robust and simple for SIF retrieval [48]. 3FLD are based on the assumption that the r and SIF vary linearly in the spectral domain considered, which overcomes the limitations given by FLD assumptions. In this way, the 3FLD-based SIF can be derived as Equation (1):

$$SIF_{in} = \frac{\left(E_{left} \times w_{left} + E_{right} \times w_{right}\right) \times L_{in} - \left(L_{left} \times w_{left} + L_{right} \times E_{right}\right) \times E_{in}}{\left(E_{left} \times w_{left} + E_{right} \times w_{right}\right) - E_{in}} \tag{1}$$

where w_{left} and w_{right} are the weight of the channel, which is proportional to the length between the longer/shorter channel and the inner channel. E and L are the downwelling irradiance and the upwelling radiance arriving at the top of the canopy, respectively. The subscripts "in", "left" and "right" represent the channels inside, at the left of and at the right of the absorption domain (758 nm, 760 nm, and 770 nm for O_2A absorption domain; 680 nm, 684 nm, and 690 nm for O_2B absorption domain), respectively.

2.5. Statistical Data Analysis

All four system were well calibrated following the radiometric calibration protocol using the reference light sources of HL-3 (Ocean Optics Inc., Dunedin, FL, USA) to calibrate the hemispherical sensor and an integrated sphere to calibrate the conical sensor in the lab, ensuring that synchronously measured incident irradiance and reflected radiance have no systematical difference obtained from these four systems. After preprocesses, such as dark current correction, quality checking, and the calculation of irradiance and radiance from digital numbers, data were then used to calculate reflectance and to retrieve SIF. In total, data observing grey reference and bare soil background, four days measuring *E. aureums* with four systems and another four days measuring lawn plot with two systems were collected and analyzed in this study.

IT and reflectance were chosen to be the indicators for the comparison of the four systems and different configurations (i.e. hemi-con and bi-hemi configurations). In the test for FOV of CC-3, the "true" footprint of hemispherical sensor (CC-3) was tested by moving a potted *E. aureums* away from the center of the sensor FOV. Diurnal patterns of instantaneously acquired SIF from different systems and configurations were also compared to evaluate the consistency of SIF obtained from a variety of devices when observing the same target, something which has not yet been reported. Statistical analyses were performed using MATLAB and Microsoft Excel software.

3. Results

3.1. Measurements of Grey Reference and Soil Background

Irradiance, radiance, and reflectance are the first things should be checked to investigate the quality of data collected from observation systems. Figure 6 shows the irradiance, radiance and reflectance measured by different systems of hemi-con configuration while the downwelling bare fiber pointing toward grey reference around noon under slightly cloudy (left volume) and changeable (right volume) conditions. The irradiance measured by these four systems showed marginal difference, while radiance from different systems varied dramatically (Appendix A.3 and Figure A3 as a complement showing the consistency of the radiance acquired from the four systems under clear and stable illumination condition). As the four systems all using sequential observation are measuring the incident irradiance first and then the reflected radiance, under changeable weather conditions, irradiance and radiance are measured asynchronously and probably under different radiation conditions, causing variations of measured reflectance. The radiation conditions were more stable at 12:04 than that at 11:06. The standard reflectance of the grey reference is 0.5 at far-red region, and reflectance measured by SI, SII, and SIII were close to this value at 12:04, but reflectance measured by all four systems were less than 0.5 at 11:06. Generally, reflectance measured by SII and SII were closer to 0.5 than the other two systems at different time, indicating the stability of SII and SIII used in fast changing weather situations.

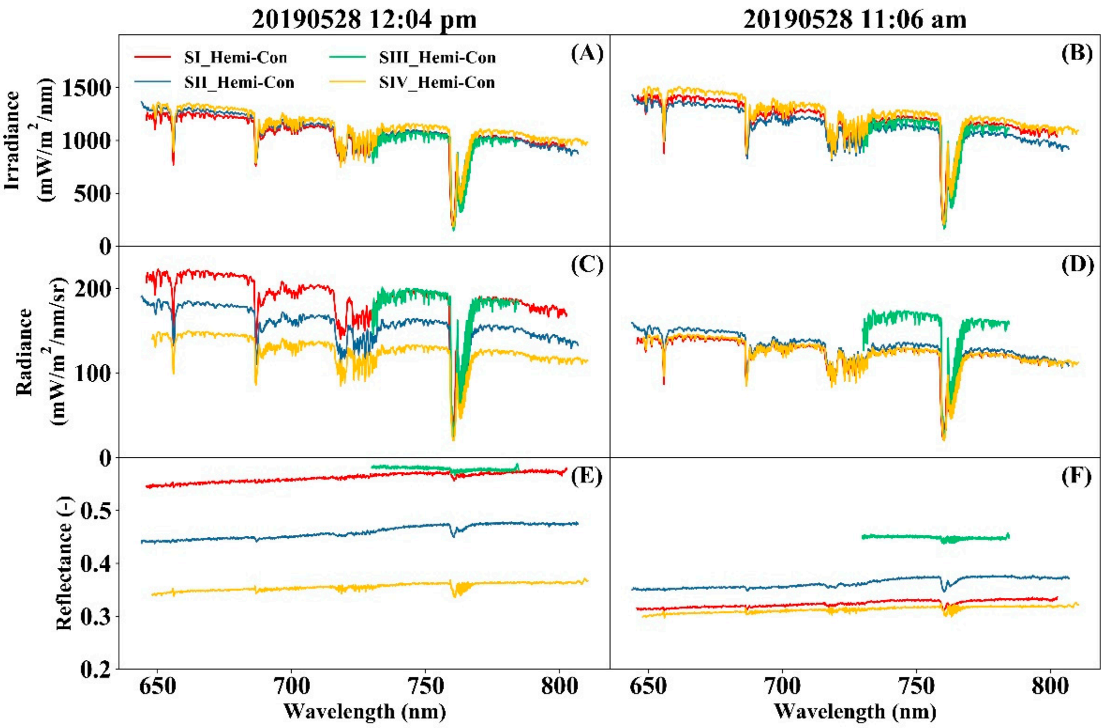

Figure 6. Irradiance, radiance and reflectance measured by different systems while the downwelling bare fiber pointing toward grey reference around noon under slightly cloudy (**A**,**C**,**E**) and changeable (**B**,**D**,**F**) conditions.

All downward pointing sensors of the four systems with the hemi-con configuration were conducted to measure bare soil ground for entire days. Integration time (IT) could be a useful factor to evaluate the efficiency of these systems. Figure 7 displays the diurnal variations of ITs of different systems measuring (A and B) irradiance and (C and D) radiance. ITs of SI and SII were much lower than the other two systems. IT of SIV was always the longest and reaching the offset maximum IT (Figure 7C) when measuring soil ground. IT of SII was around half of that of SI, showing high observation efficiency, which was also the reason for SII having high SNR.

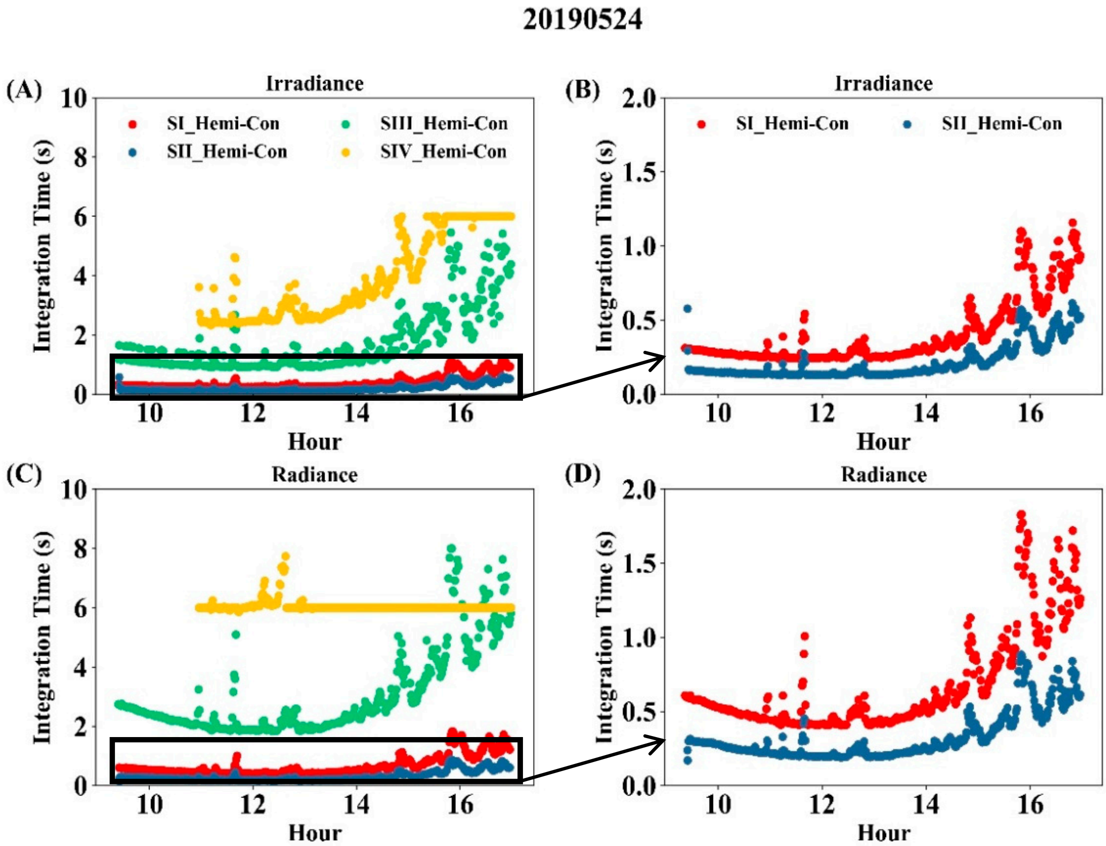

Figure 7. Diurnal variations of integration time (**A**,**B**) irradiance and (**C**,**D**) radiance of different systems with hemi-con configuration while the downward bare fiber pointing toward bare soil background. The right volume is the magnification of integration times (ITs) of systems I and II (SI and SII).

The main difference between hemi-con and bi-hemi configurations is the different viewing geometry as that the hemi-con measurements can be taken by observing the canopy at nadir or off nadir, while both nadir and off-nadir contribute to the bi-hemi measurements but in different weights [28]. Reflectance of soil ground measured from SI, SII and SIII of hemi-con (Figure 8A) and bi-hemi (Figure 8B) configurations of are shown in Figure 8. Reflectances measured by different systems had marginal difference by the bare fiber for hemi-con configuration, and those from the cosine corrector for bi-hemi configuration were also similar. Even though measurements of the downward sensor with bare fiber and cosine corrector have different viewing geometries, the soil was generally homogeneous, such that the reflectances measured by the bare fiber and cosine corrector were almost not affected by different viewing geometries.

3.2. Measurements of Vegetation Canopy

Both hemi-con and bi-hemi configurations for SI, SII and SIII were conducted to measure vegetation canopy during the days, while only SIV of hemi-con configuration was setup as a reference. The upwelling hemispherical sensors of the three systems and the conical sensor of SIV were mounted at different height but had almost the same FOV. Similar to measuring soil ground, diurnal variations of IT of the four systems with conical sensors (9th May) and with hemispherical sensors for the upwelling channel (12th May) are shown in Figure 9. On 9th May, when the downward pointing sensors of all systems measured with conical sensors, ITs of SI and SII were much lower than the other two, and the IT of SII was about half of that of SI, which was same as measuring the bare soil ground. On May 12th, when the downward sensors of SI, SII, and SIII were equipped with cosine correctors, all ITs became longer. And IT of SII was closer to but still much lower than that of SIV compared to the results on May 9th. Similar patterns have been found when the upwelling hemispherical sensors of the three systems and the conical sensor of SIV were mounted at the same height but had different fields of view, as shown in Figure A5. Whether the upwelling sensor equipped with cosine corrector or not, SII always has the shortest IT, i.e., the greatest efficiency.

Figure 10 showed the irradiance, radiance and reflectance of SI and SII when downward pointing sensors (Figure 10A,B) were conical sensors and (Figure 10C,D) were hemispherical sensors measuring vegetation canopy. The irradiance and radiance measured by the two systems were very close. Hence, the reflectance calculated from these two systems was also quite similar. The small fluorescence peak of reflectance at 687 nm could be observed from both SI and SII. In contrast, the fluorescence peak of reflectance at 760 nm was clear from SII while that from SI had an abnormal vibration, which was possibly due to spectral shifting caused by the impalpable difference between the two paths of the splitter fiber. Whether it was downward pointing conical sensors or hemispherical sensors, the shapes of reflectance had no difference. SII shows its advantage of avoiding spectral shifting and being able to measure "perfect" shape of vegetation reflectance.

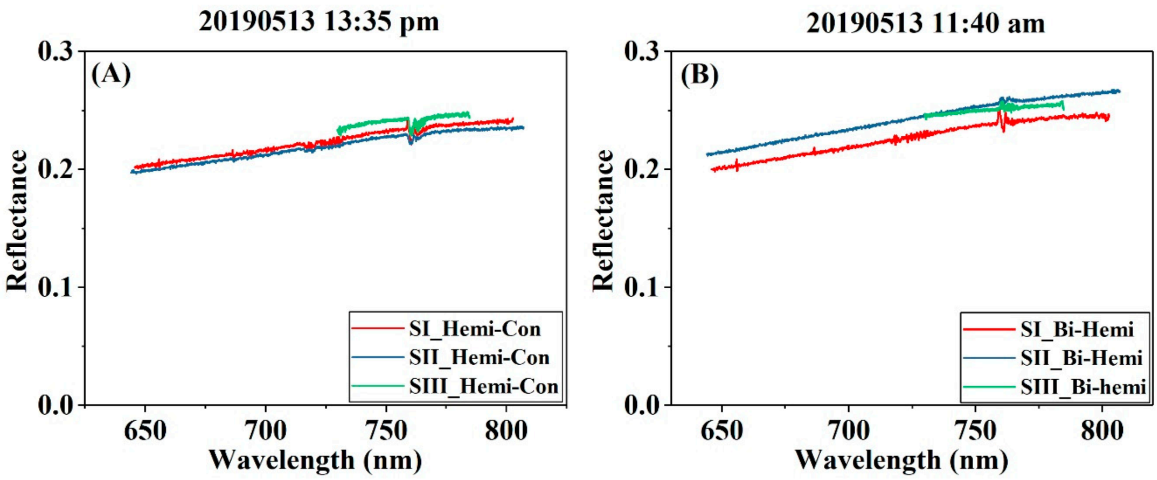

Figure 8. Reflectance of different systems with (**A**) hemi-con and (**B**) bi-hemi configurations while the upwelling sensors pointing toward bare soil background.

Reflectance measured by the four systems of hemi-con and bi-hemi configurations at different (Figure 11A,C) and the same heights (Figure 11B,D) were displayed in Figure 11. All reflectances were measured under similar illumination condition. Figure 11A,B shows differences among reflectance from four systems, which were similar to those shown in Figure 6, probably owing to the different IT of the four systems and asynchronous measurements of incident irradiance and reflected radiance. Either at different or the same heights, reflectance measured with hemispherical sensors (Figure 11C,D) exhibited obvious differences to those measured with conical sensors (Figure 11A,B), with relatively higher reflectance in red region and lower reflectance in far-red region. Even though the FOV of the hemispherical sensor was theoretically covered by vegetation, it seems the reflectance measured by hemispherical sensor contains the signal of background. To test the usefulness of cosine corrector in measuring reflected radiance of vegetation, we conducted another experiment to clarify the "real" FOV of it.

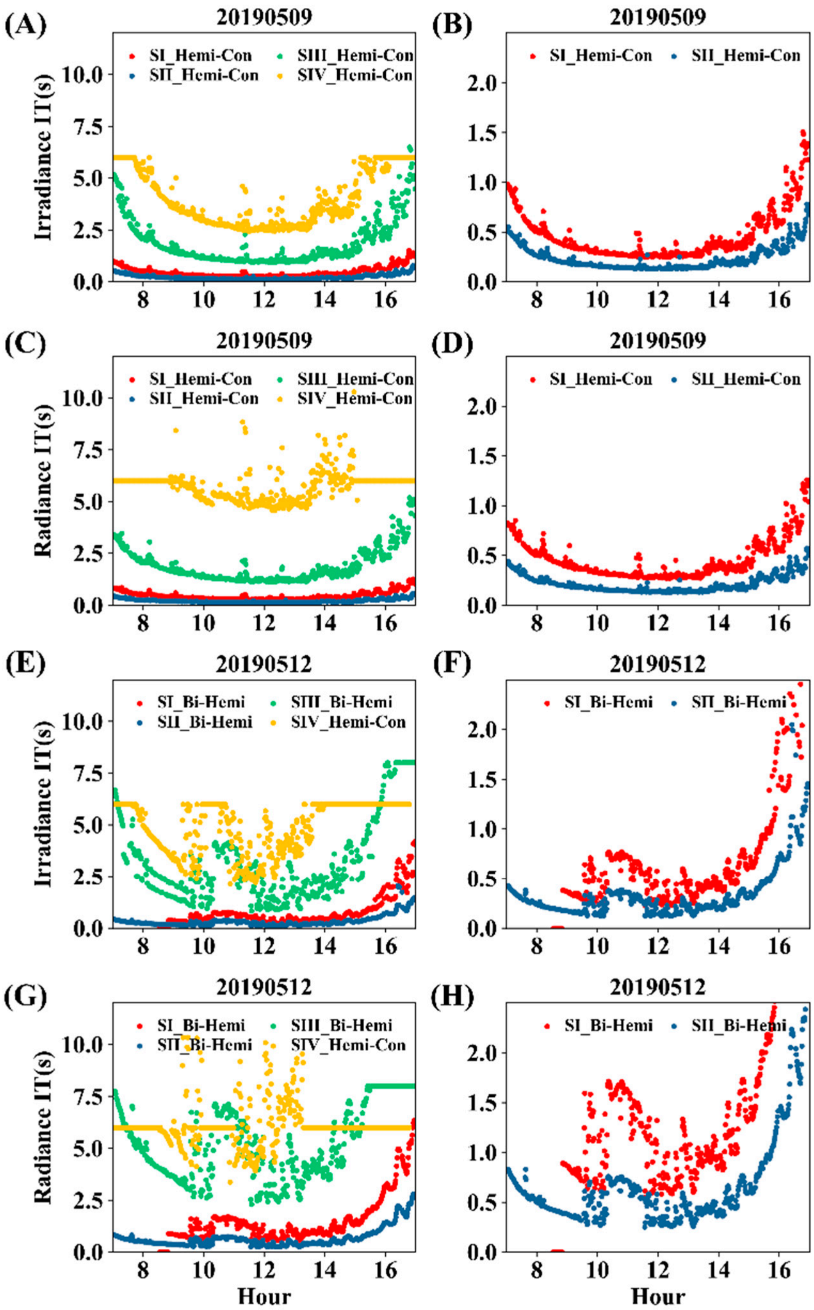

Figure 9. Diurnal variations of integration time of different systems of (**A**–**D**) hemi-con and (**E**–**H**) bi-hemi configurations (SIV of hemi-con configuration as a reference) while the upwelling sensors pointing toward vegetation with almost same field of view (different viewer height). The right volume specifically shows the integration times (ITs) of SI and SII.

As described in Section 2.3 for the test of CC-3 FOV (Figure 6), two pots of *E. aureums* were placed under the horizontal center (origin shown in Figure 12) of the hemispherical sensor FOV at first with 1.0 m vertical distance between the sensor and the top of the canopy, and was moved away from the center at a 0.2 m step. Figure 12 shows the variations of SIF, reflectance at 760 nm and NDVI with the distance between *E. aureums* and the center. When *E. aureums* was moved away from the FOV center, SIF, reflectance at 760 nm, and NDVI all dramatically decreased with an increase of distance. Once the distance was larger than one meter, the decreases of the three parameters with distance were slackened. Reflectance at 760 nm remained invariant since the distance reached 1.4 m, while SIF and NDVI kept slowly decreasing until SIF became negative and NDVI turned to be steady around 0.05

when *E. aureums* was pulled 2.0 m away from the FOV center. The underlying picture indicates the vegetation canopy and the transparency of the rings represents the contributions of different places of the canopy to the SIF signal captured by the cosine corrector. The theoretical radius of the footprint of the cosine corrector simulated by Liu et al. [43] should be 2.7 m above the canopy here. Our findings suggested that the measured SIF signal was limited at 2.0 m the same as NDVI behaved. This result also indicates the far-red SIF signal of vegetation measured by the spectrometer is beyond the range expressed by reflectance at 760 nm when the reflectance was already invariant before that distance.

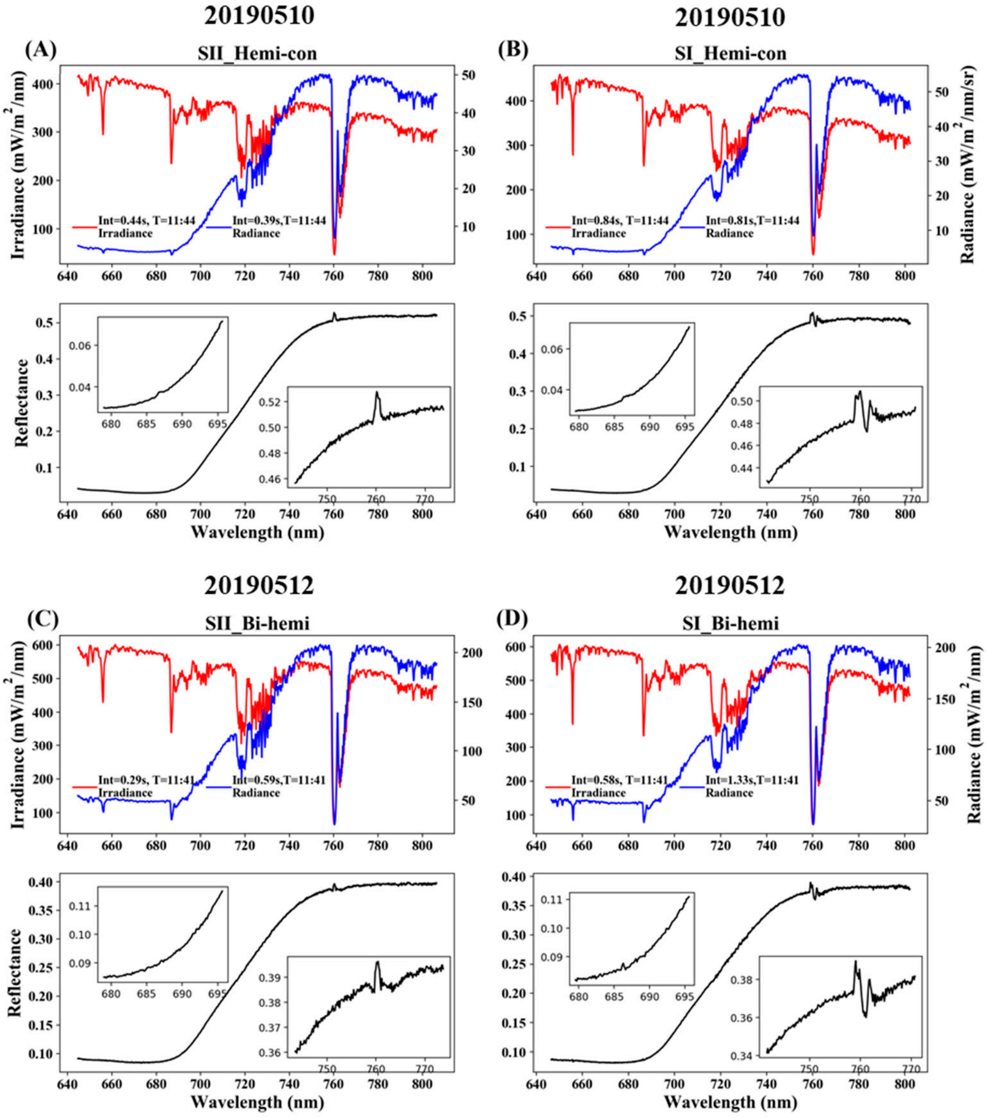

Figure 10. Irradiance, radiance and reflectance measured by the splitter (SI) and prism systems (SII) of (**A**,**B**) hemi-con and (**C**,**D**) bi-hemi configurations while the upwelling sensors pointing toward vegetation.

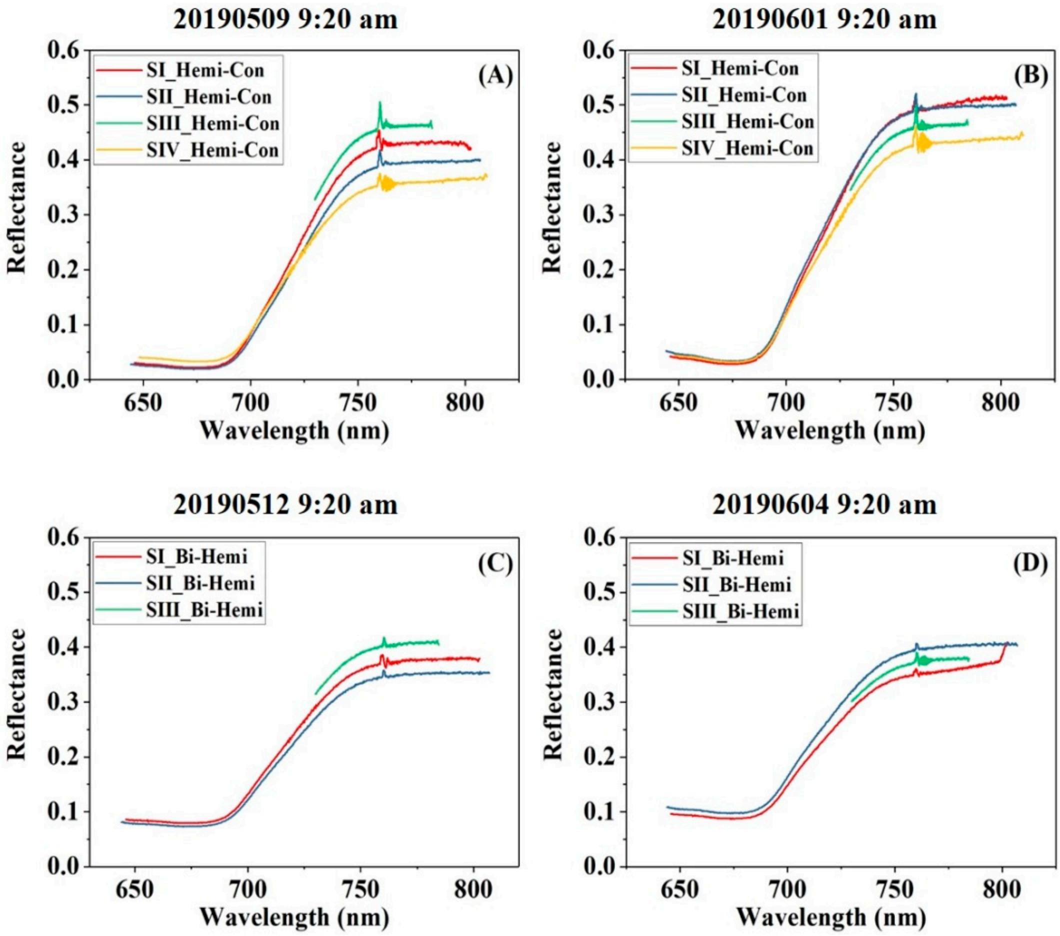

Figure 11. Reflectance measured by the four systems (**A**,**B**) of hemi-con and three systems (**C**,**D**) of bi-hemi configurations while the upwelling sensors pointing toward vegetation. (**C**) shows the data that the upwelling sensors of the three systems have almost same field of view as the conical sensor of SIV (different viewer height), while (**D**) shows that those three upwelling sensors were mounted at the same heights as that of SIV (different field of view).

3.3. Retrievals of SIF from Four Systems

SIF retrieved from the four systems of hemi-con configuration measuring the plot of *E. aureums* were compared (Figure 13). Diurnal variations of SIF shown in Figure 13A,C were acquired under slightly cloudy but stable sky conditions and those in Figure 13B,D were acquired under changeable cloudy conditions. All far-red SIF obtained from four systems exhibited minor differences as all sensors have the equivalent FOV and measured the same spot of the canopy with synchronously changed sun-viewer geometry across the day. On May 9th, red SIF obtained from SIV were a little lower than those from another two systems under slightly cloudy conditions (Figure 13C), probably due to its longer IT (Figure 9) and lower SNR (Figure A4) which affect the detection of red SIF signal, which is much weaker than far-red SIF signal. These results indicate that different constructions and spectrometers used in the four systems have a rare influence on the retrieval of far-red SIF, but may affect retrieval of red SIF if the SNR is not high enough (usually > 1000:1), and a new-built prism system (SII) is effective to acquire a SIF signal.

As SIFprism (SII) had proven able to obtain SIF as other systems, we specifically equipped the upwelling sensor with a cosine corrector (CC-3) to measure the hemispherical radiance of the canopy and used the FLoX (SIV) of hemi-con configuration as a reference. Downward sensors of SII of bi-hemi configuration and SIV of hemi-con configuration were set to measure a field of grassland, of which canopy was very homogeneous and large in respect to the FOV of upwelling hemispherical fiber. Diurnal variations of retrieved far-red and red SIF from the two systems showed quite similar values and features both at the same (Figure 14A–D) and different heights (Figure 14E–H) under different weather conditions, varying with changes of photosynthetic active radiation (PAR, shaded area) measured by a sunshine sensor BF5 (Delta-T Devices Ltd., Cambridge, UK). Either the upwelling sensors of the two systems set at the same or different heights, the footprints and viewing geometry of hemispherical sensor and conical senor were different, proving that this difference does not affect the variations of SIF signal in the homogenous field. Data shown in this figure were filtered according to the criteria of quality-control presented by Cogliati et al. [12], such that there were some small gaps while there were two big gaps in Figure 14A,C due to system failure. On these four days, whether under clear or cloudy conditions, the weather changed very fast, and SII was able to reveal the influence of changeable illumination on SIF observation as it has a shorter IT than that of SIV, and is consequently able to reject poor-quality data.

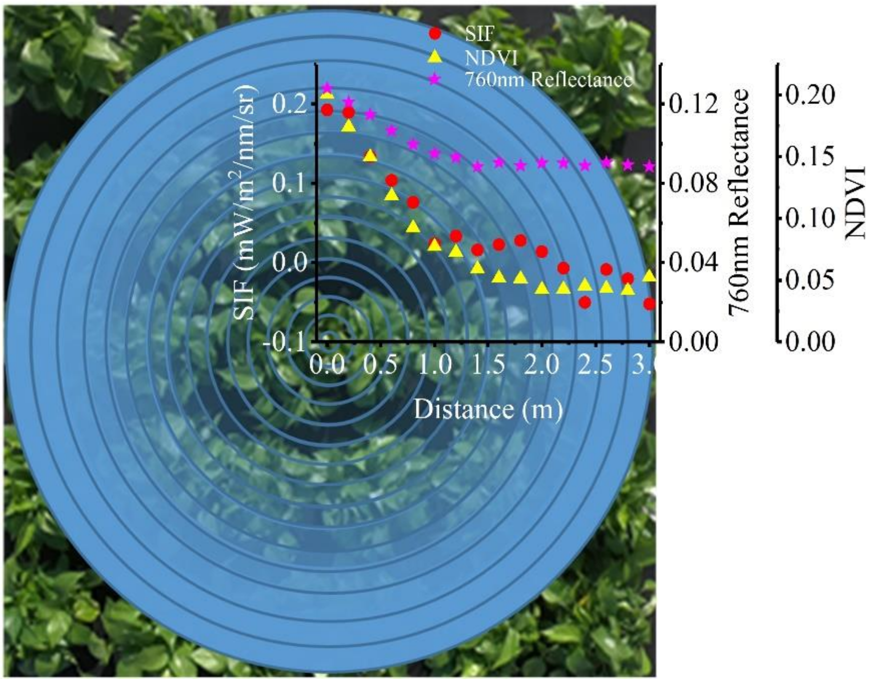

Figure 12. Variances of far-red solar-induced chlorophyll fluorescence (SIF), reflectance at 760 nm and normalized difference vegetation index (NDVI) with the horizontal distance between the plant and the horizontal center of the view of cosine corrector.

As shown in Figure 11, the reflectance measured by SI, SII, and SIII of hemi-con configuration were different from those of bi-hemi configuration when measuring *E. aureums* plot, of which canopy was considered as heterogeneous due to background effects. When the SIV of the hemi-con configuration was used as a reference, the values of far-red SIF retrieved from the other three systems were much lower than that from FLoX (SIV) on two days under different weather conditions (Figure 15A,B). Meanwhile, diurnal patterns of far-red SIF from SIV were significantly different with that from systems of bi-hemi configuration which did not have clear diurnal patterns. On the contrary, diurnal courses of red SIF retrieved from the three systems (SI, SII and SIV) exhibited a non-significant difference when the upwelling sensors were mounted at different heights but had general same FOV (Figure 15C) and a little higher values of SIF from SIV than the other two when the upwelling sensors were mounted at the same height (Figure 15D). These results indicate that, for a heterogeneous canopy, different configurations affect the observation of red and far-red SIF in different ways owing to different footprint sizes, viewing geometries, and radiative transfer regimes of different bands, which will hereafter be specifically discussed.

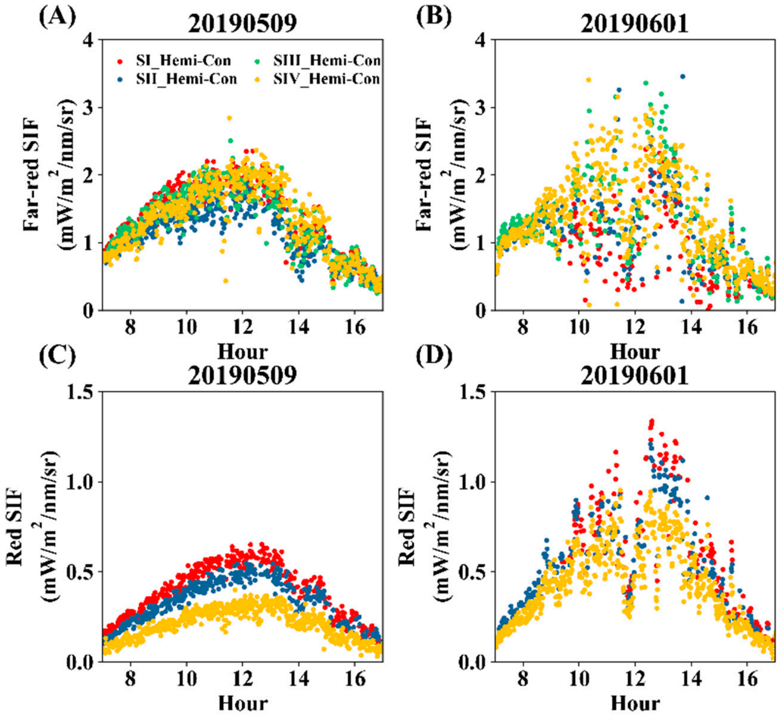

Figure 13. Diurnal variations of retrieved far-red and red SIF from measurements by the four systems of hemi-con configuration while the upwelling sensors pointing toward non-continuous vegetation one two days (**A**,**C**) under slightly cloudy but stable sky and (**B**,**D**) under changeable cloudy sky) conditions.

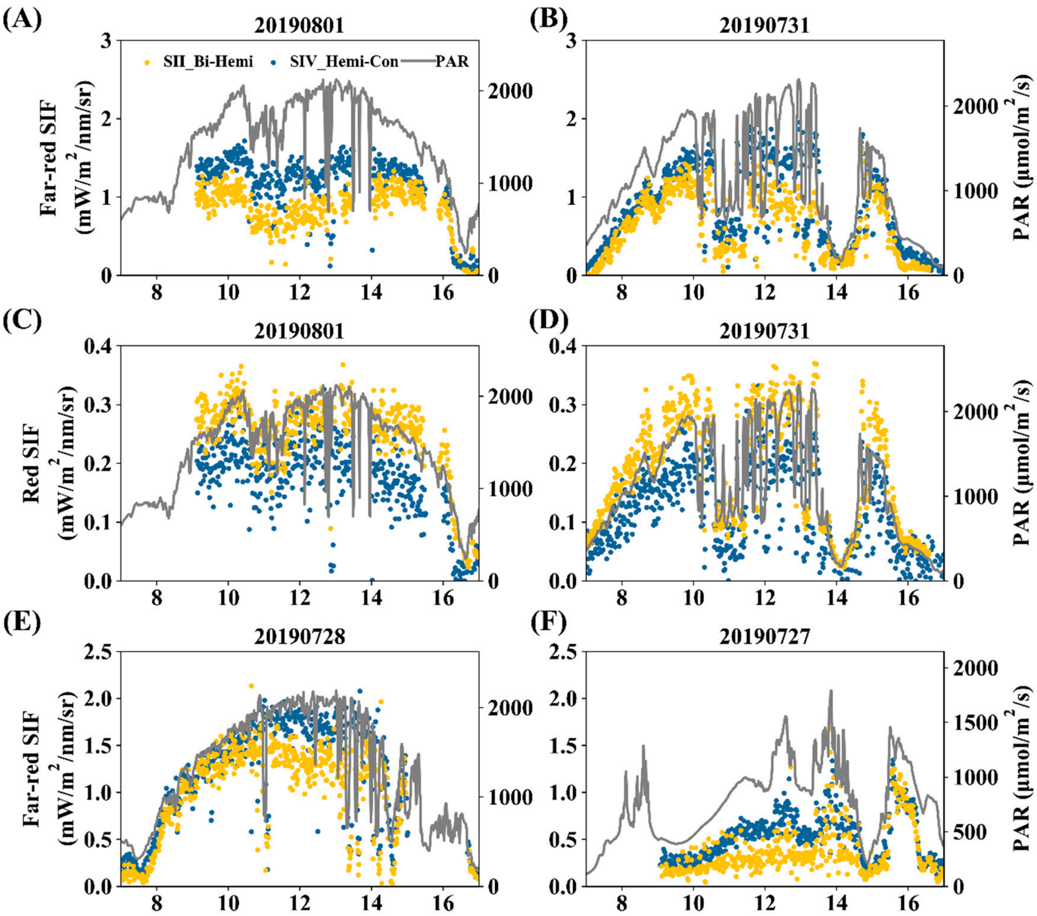

Figure 14. *Cont.*

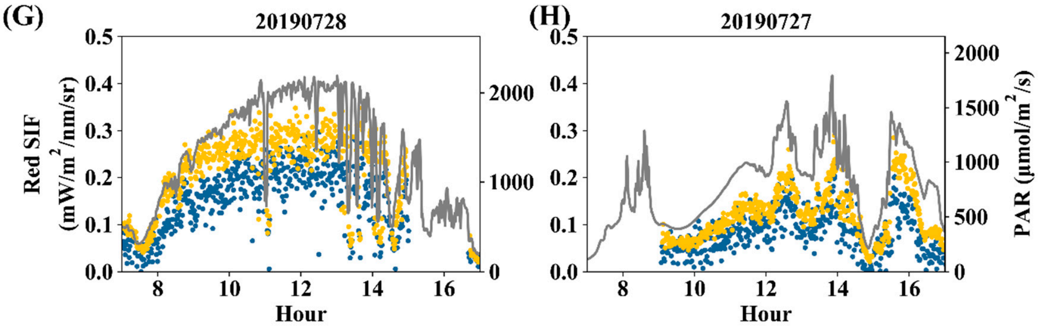

Figure 14. Diurnal variations of retrieved far-red and red solar-induced chlorophyll fluorescence (SIF) from measurements by SII of bi-hemi configuration and SIV of hemi-con configuration while the upwelling sensor pointing toward continuous vegetation at (**A**–**D**) the same and (**E**–**H**) different heights under different weather conditions (left volume is under clear sky and right volume is under cloudy sky). Shaded areas represent diurnal course of photosynthetic active radiation (PAR) measured by a sunshine sensor BF5.

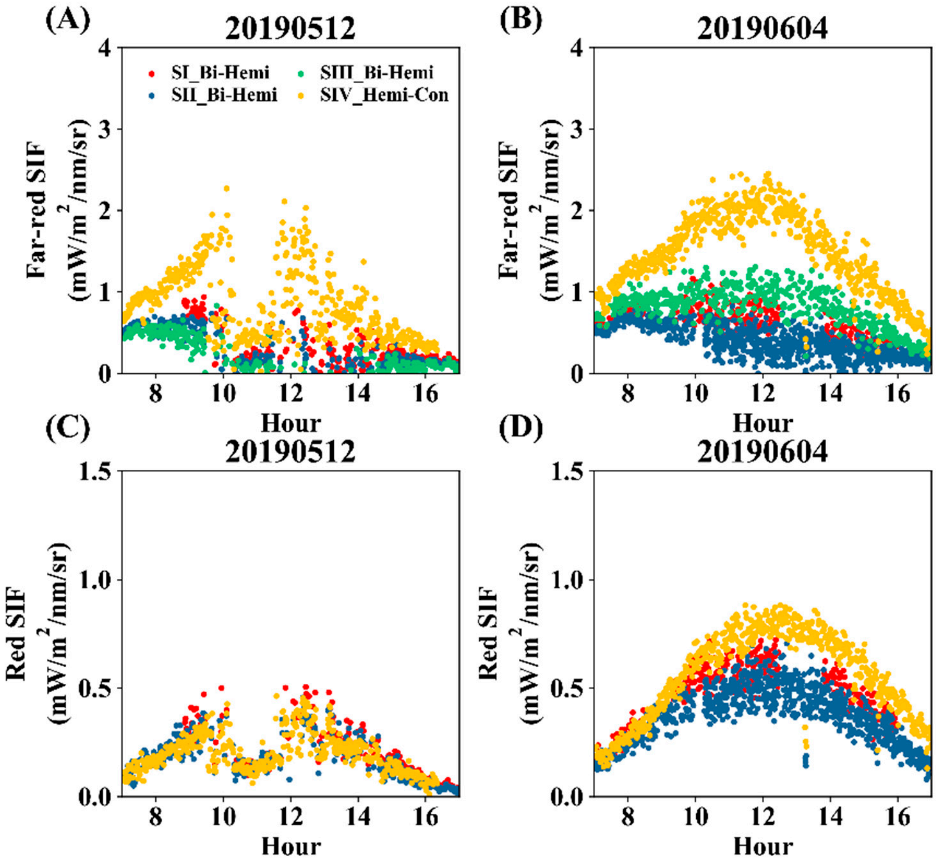

Figure 15. Diurnal variations of retrieved far-red and red solar-induced chlorophyll fluorescence (SIF) from measurements by the four systems of bi-hemi configuration while the upwelling sensors pointing toward discontinuous vegetation under different conditions. (**A**,**C**) show the data of upwelling hemispherical sensors and conical sensor set at different height, and b and show those set at the same height.

4. Discussion

4.1. Comparison of Different SIF Systems

Several types of ground-based systems have been employed for continuously monitor vegetation SIF during the past few years. Up to now, the most acceptable construction of this kind of system (e.g., FLoX, FluoSpec2, Photospec and FAME) integrates spectrometers from Ocean Optics Inc.: FLAME/HR2000+, QEPro, with splitters fiber and inline TTL for sequentially measuring and switching between solar irradiance and vegetation radiance [18,23,27]. Our new built SIFprism was derived from a prism system developed by Ari Kornfeld and Joe Berry (Department of Global Ecology, Carnegie Institution for Science), and the part of splitter fiber and inline TTL was replaced with a rotary prism box. For the first time, we tested four different constructed systems (SI–SIV) of different configurations to analyze the feasibility of monitoring SIF acquired from different sites using different devices across the world. SI and SIII were built by our team based on existing constructions, and SIV (FLoX) was a commercial product we bought, all of which could be treated as existing well-accepted SIF observation systems. SII was newly developed and built, which was specifically compared with the other three systems.

The IT of four systems measuring soil ground (Figure 7) and vegetation (Figures 9 and A4) were compared. The spectrometer with a larger spectral range (650–800 nm) or slit (25 um) has a larger FWHM but higher light sensitivity. Therefore, the ITs of SI and SII were much shorter than those of the other two. Prism can reduce more than 50% the light loss through splitter fiber and inline TTL as IT of SIFprsim (SII) was about half of SI whether the upwelling sensors were equipped CC-3 or not. A shorter IT could help to improve the SNR (Figure A2) and enable the almost simultaneous measurements of downwelling and upwelling radiation to minimize the temporal mismatch between them as much as possible [35]. This will also be helpful for high-quality data acquisition under fast changing weather conditions and in the precision of SIF retrieval [34].

When four systems were setup to measure grey reference under fast changeable (in seconds) radiation, irradiances from four systems were consistent while radiances and reflectance were different (Figure 6). As these four systems are well radiometric calibrated, there are two possible reasons causing this result. The sampling temporal interval was set as one minute for all the four systems, thus the irradiances from the four systems were almost synchronously. However, due to different ITs, the sequential acquisition of radiances from them was non-synchronous. A shorter IT of SII makes it more relatively simultaneously measure irradiance and radiance comparing to other systems. Another potential reason is that even the four upwelling sensors were bound together and pointed to the grey reference, and they may measure different spots of the grey reference of different reflected radiance, which is hard to avoid.

Spectral shifting is an obstacle to guaranteeing the precision of SIF measurement [29,35]. The prism system is able to avoid spectral shifting as all light from two channels penetrating through unique optical path into spectrometer without light mixing via the splitter fiber. This issue for the system with splitter fiber is inevitable and hard to be resolved. One possible way is keeping straight and slack in the joint place of the splitter fiber, which may need many tests to get a 'right' shape of reflectance. An alternative option is to perform wavelength calibration respectively for each optical path and to recalculate the wavelength for each band of the two channels [14,32].

Solar irradiance and canopy radiance measured precisely at the same wavelengths and with the same accuracy is an ideal case for SIF observation, which is unachievable with exist technology for now [34]. Nevertheless, red and far-red SIF from the four systems of hemi-con configuration varied parallel over the day even under variable weather conditions (Figure 13). Even though the accuracy of SIF retrieved from these systems is unable to be assessed, these results prove that all these constructions of SIF-measuring instruments are effective to monitor in situ SIF.

4.2. Comparison of Hemi-Con and Bi-Hemi Configurations

When the upwelling sensor was equipped with a diffuser (CC-3), the IT of this sensor may be doubled due to the light attenuation of the diffuse material of the cosine corrector. Even so, the ITs of SI and SII were still much lower than SIV (as reference) (Figures 7 and 9). Therefore, the most affected by the bi-hemi configuration are vegetation reflectances and SIF.

Reflectances measured with the hemi-con and bi-hemi configurations were indistinguishable when the target was soil ground (Figure 8). However, the differences of reflectance are notable when the target was the plot of *E. aureums* as the hemispherical reflectance was higher in the visible region and lower in the near infrared region than the conical reflectance (Figure 11). This is similar with the feature that the soil reflectance is also higher in the visible region and lower in the near infrared region than the vegetation reflectance, indicating that soil ground signals may be captured by hemispherical sensor when measuring the small *E. aureums* plot (only 2.5×2.5 m^2). As the soil ground is homogeneous and continuous while the vegetation plot is heterogeneous and discontinuous at this small scale, different viewing geometries and footprints of hemispherical and conical sensors resulted in the differences of vegetation reflectance even though more than 90% of the conical signal is from the vegetation canopy [43], but also had a rare influence on ground reflectance (Figure 16). This result impelled us to test what the footprint of CC-3 may truly be.

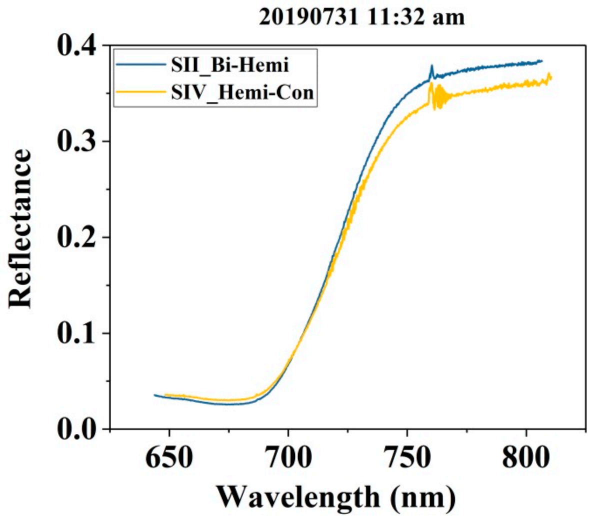

Figure 16. Reflectance of grassland measured by SII of bi-hemi configuration and SIV of hemi-con configuration.

The photon-receiving part of CC-3 is built 1–2 mm below the rim, meaning that the actual FOV is definitely less than 180°. Liu et al. [43] reported that 90% of the total radiation captured by CC-3 is from an FOV of 144°, of which the radius is approximately triple the sensor's height from the canopy. By moving the vegetation target away from the center of FOV, we found that far-red SIF signal became negative before the radius of FOV reached triple of the sensor height (Figure 12). Meanwhile, the far-red SIF of the plot of *E. aureums* measured with bi-hemi configuration were much lower than those measured with hemi-con one (Figure 15) but were consistent when measuring a plot of grassland (Figure 14). This is probably due to multiple scattering of heterogeneous canopy in the far-red region causing a mismatch between estimated and real footprints. Furthermore, the actual viewing geometry may be different with the assumed one when hemispherical and conical sensors were set at different heights (Figure 15A). Therefore, considering the shape of canopy reflectance of *E. aureums* (Figure 11), far-red SIF of this kind of heterogeneous canopy is interfered with by the soil ground signal. However, the case is different for red SIF, which is highly reabsorbed by the canopy but rarely multiple scattered thus measured red SIF is mainly from top of the canopy. As long as the assumed footprints of upwelling hemispherical and conical sensors were the same (Figure 15C), red SIF values were the same even the viewing geometry were different. While all upwelling sensors were set at the same height, red SIF from conical sensor was larger than others as the conical sensor has a smaller footprint but larger probability of seeing more sunlit leaves in its FOV when the solar zenith angle is small (around noon) (Figure 15D).

4.3. Implications for Future Work

Our newly built prism system (SIFprism) showed its consistency with commercial products (FLoX, SIV) and widely used systems (SI and SIII) for measuring reflectance and deriving SIF for a homogeneous canopy. Short IT enables SIFprism system to be used for changeable weather condition and to obtain high-precise SIF measurements [34]. However, the essential point of the prism system, whether it can be reliably used for long-term field operation, is the repeatability of the rotation of the prism to ensure the two optical paths are stable. As a newly built system, it still needs to be run in situ for a long time to investigate its stability. The prism system is suitable for measuring hemispherical canopy radiance taking the advantage of short IT, even CC-3 may dampen more than half of the light density.

The bi-hemi configuration has an advantage in that it is able to capture signals from a large footprint area even the upwelling sensor is not mounted at high altitude. For monitoring photosynthesis derived from eddy covariance (EC) measurement using EC tower-based SIF measurement, mismatch between the footprints of these two measurements is a critical issue must be considered [34]. The footprint of EC measurement, which is usually tens of times the distance between the sensor and the canopy, is designed to represent the average condition of the canopy, no matter whether the canopy is homogeneous or heterogeneous. The SIF system of hemi-con configuration is probably suitable for homogeneous canopy but is hard to be representative for heterogeneous canopy when its diameter of FOV is still less than 10 m even the sensor is mounted 20 m above the canopy. In contrast, for upwelling channel, hemispherical sensor has a much larger FOV than conical sensor (almost 7 times) [43] and is better at matching an EC footprint. Therefore, the bi-hemi configuration can be well used above a heterogeneous canopy to acquire average information. But this configuration is non-preferable for a discontinuous canopy, such as small plots in the controlling experiment, needing to make sure the upwelling signal is not beyond the canopy. Another important thing is that proper atmospheric correction is necessary for SIF retrieval with the use of a cosine corrector to collect vegetation radiation due to long light path at large view angles [30].

5. Conclusions

In this study, we conducted a field experiment for SIF measurements from four different observation systems (SI and SIII built from existing construction, SII newly built and SIV bought as a commercial product) together to find out whether SIF from different systems are comparable. We also investigated the impacts of different FOV on the SIF observations. IT, reflectance, and SIF retrieved from different systems with hemi-con and bi-hemi configurations were compared. Generally, the IT of spectrometer with large spectral range or a large slit is much shorter than the opposite one. We have demonstrated that the newly built prism system (SIFprism, SII) has the shortest IT and highest SNR giving credits to less light loss than splitter fiber and higher efficiency nearly two times of the construction using TTL and splitter fiber (SI). This advantage is also helpful to improve the data quality for SIF retrieval, especially where the weather is changeable. Reflectance collected from different systems showed small difference when measuring different targets, and correspondingly, diurnal courses of SIF (either red or far-red SIF) retrieved from different systems displayed marginal difference, either with hemi-con or bi-hemi configuration when (only) measuring homogeneous (continuous) vegetation canopy (grassland), demonstrating the consistency of different systems for spectra and SIF observations. We found that, however, when the target is heterogeneous (discontinuous) as in the *E. aureums* plot, the values and diurnal pattern of far-red SIF derived from systems (SI, SII and SIII) with a bi-hemi configuration were obviously distinct from those derived from the system (SIV) with a hemi-con configuration.

This is probably due to the different footprint sizes and viewing geometries between hemispherical and conical upwelling sensor attributed by multiple scattering at the far-red region. A larger FOV of the hemispherical sensor than conical sensor is suitable for the observation of a heterogeneous canopy and better matches the footprint of EC measurements, but was restricted for observation of a discontinuous canopy (such as small plots of control experiment). Our results highlight the importance of conducting the bi-hemi measurements for SIF retrievals to integrate with EC flux measurements which have a larger footprint. This study is of more technical than scientific importance, but it may nevertheless serve further studies on the comparison of SIF acquired from various sites with different observation systems.

Author Contributions: All of the authors conceived of, designed and performed the laboratory and field experiments.; Writing—Review & Editing, Q.Z., X.Z. and Y.Z.; Funding Acquisition, Q.Z. and Y.Z.

Funding: This research was funded by National Natural Science Foundation of China, grant number: (41701393 and 41671421); by International Cooperation and Exchange Programs between NSFC and DFG grant number: (41761134082), by Natural Science Foundation of Jiangsu Province for Youth grant number: (BK20170641); and by China Postdoctoral Science Foundation, grant number: (2018T110477).

Acknowledgments: We gratefully acknowledge the support from Ari Kornfeld and Joe Berry (Department of Global Ecology, Carnegie Institution for Science) for helping us to build the prism system. We further acknowledge our group members for their help in the field work.

Conflicts of Interest: The authors declare no conflict of interest.

Appendix A.

Appendix A.1. Interface of NJUspec Controller

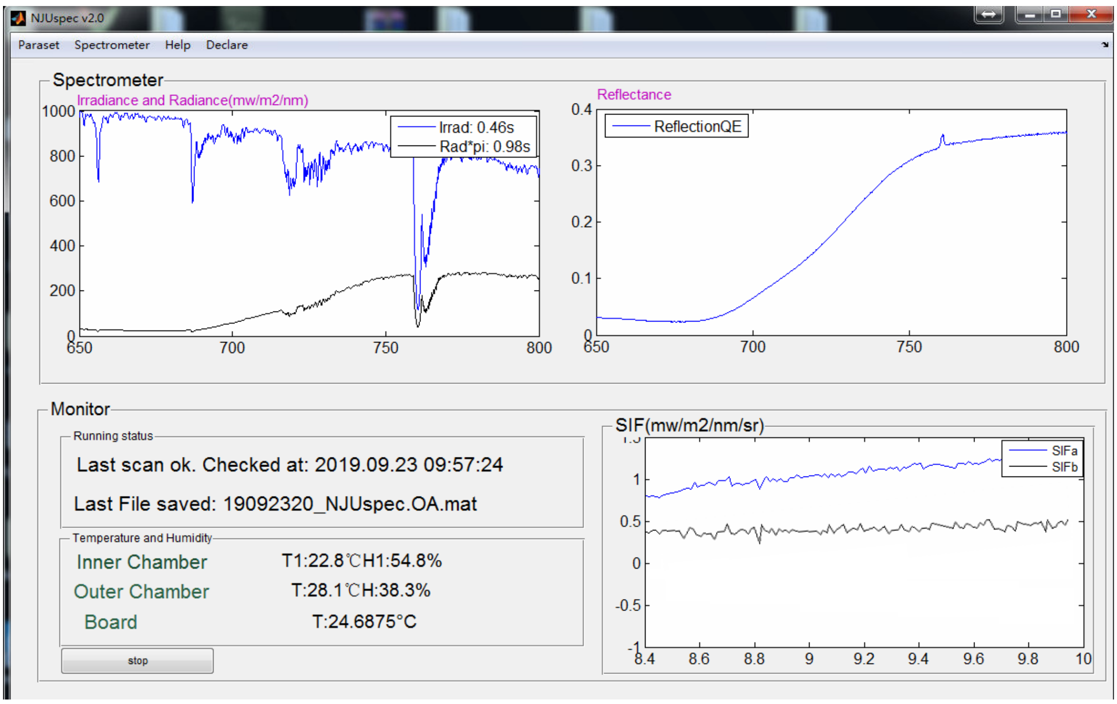

Figure A1. Software interface of NJUspec Controller. The box in the upper-left of the interface displays the values and shapes of radiance and irradiance, and their integration time. The box in the upper-right of the interface displays the reflectance of measurement targets. The bottom left of the interface displays the local time, the name of last saved file name, the temperature of inner chamber, outer chamber and motherboard, and the relative humidity of inner chamber and outer chamber. The box in the bottom right of the interface displays the solar-induced chlorophyll fluorescence (SIF) values.

Appendix A.2. Inner Environmental Conditions of SIFprism

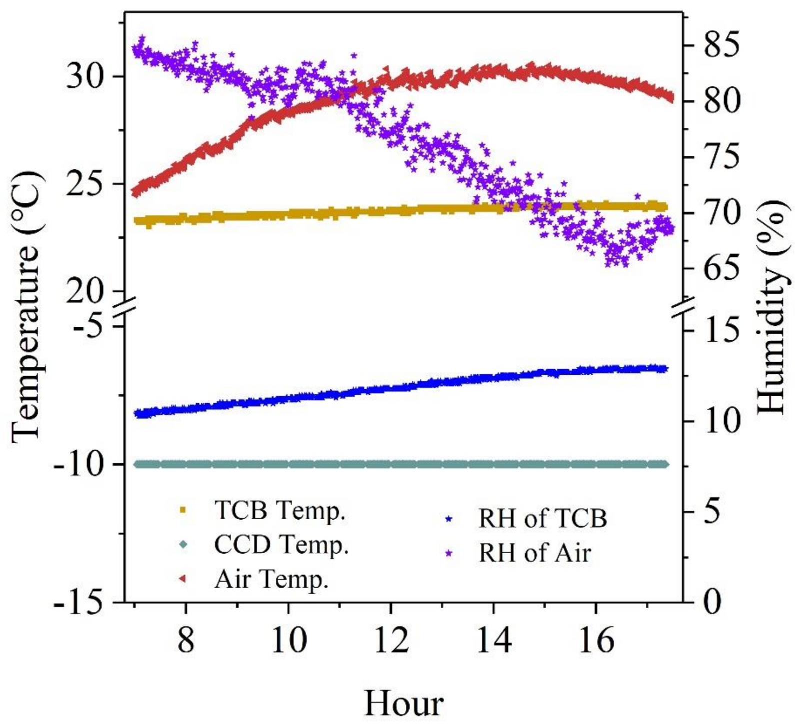

Figure A2. The temporal dynamics of temperature (Temp.) and relative humidity (RH) of Temperature Control BOX (TCB), Charge Coupled Device (CCD) and air.

Appendix A.3. Radiance of Four Systems Acquired under Stable Illumination Condition

Radiance observed from 11:40 to 12:00 on May 9th when illumination condition was quite stable and shown in Figure A3. Radiance acquired from the four systems varied slightly with changes in illumination and were similar but with minor difference due to small different field of view of each system measuring heterogeneous canopy.

Appendix A.4. Estimation of Signal to Noise Ratio (SNR) of the Four Systems

Based on measurements of grey reference, the spectral signal to noise ratio (SNR) of the four systems were calculated [49] and shown in Figure A4.

$$\mathrm{SNR} = \frac{S}{N} = \frac{R_{DN,total} - R_{DN,dark}}{\left(\sigma^2\left(R_{DN,total}\right) + \sigma^2\left(R_{DN,dark}\right)\right)^{1/2}} \tag{A1}$$

where $R_{DN,total}$ and $R_{DN,dark}$ represent total measured signal and dark current, respectively. DN means digital number, and σ is the standard deviation. The total signal refers to the average of repeated measurements of a grey reference panel (Spectralon, Labsphere, NH, USA) at noon under a relatively stable sky condition. Ambient light is ensured during the measurements to guarantee the relatively high radiance levels, which is usually present in naturally illuminated scenes.

During the measurements (around 15 min), 10–20 spectra data for each system were acquired. Generally, SII has the highest SNR while SIV has the lowest SNR, probably due to more incident light input into the spectrometer of SII using 25 um slit than that of SIV using 5 um slit.

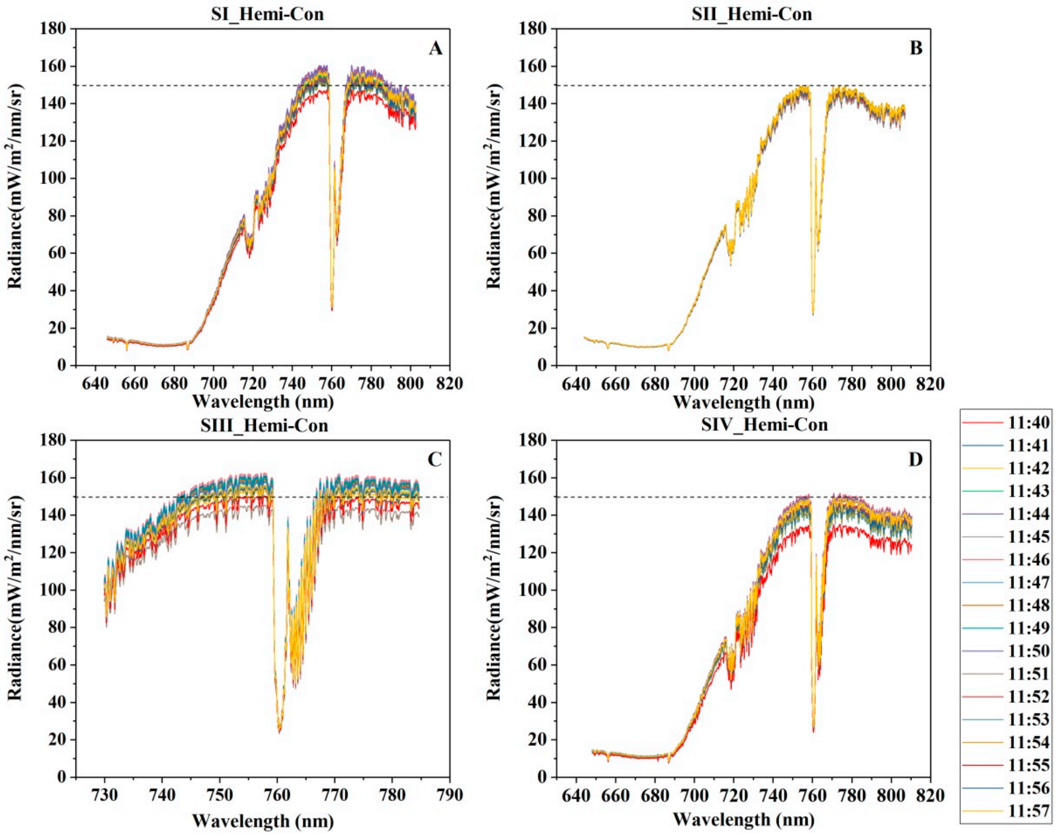

Figure A3. Radiance of four systems acquired under stable illumination condition. The dashed lines represent irradiance value of 150 mW/m^2/nm.

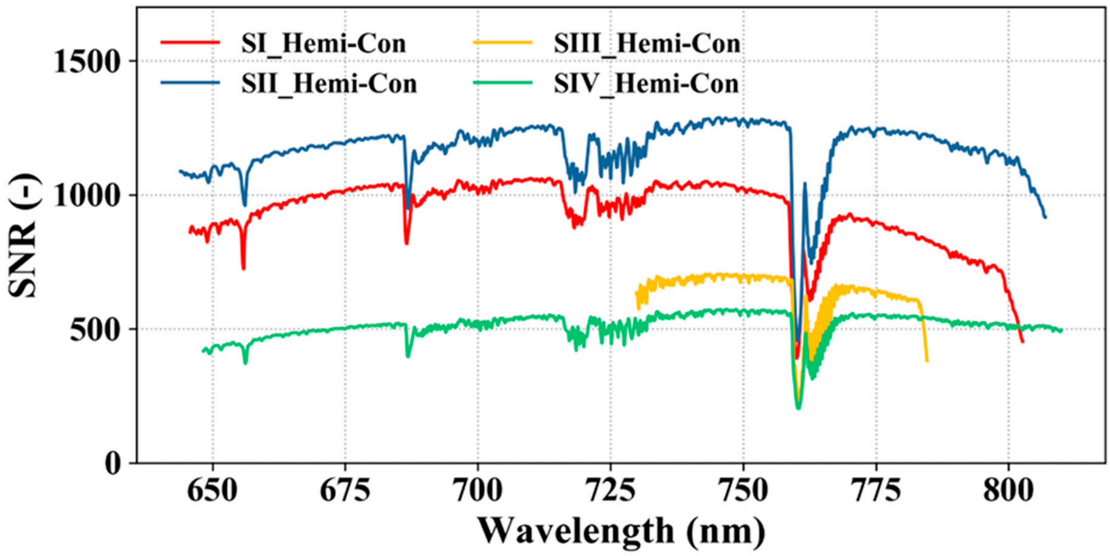

Figure A4. Spectral signal to noise ratio of four systems.

Appendix A.5. Estimation of Signal to Noise Ratio (SNR) of the Four Systems

Similar to Figure 10, when downward sensors with bare fiber and with cosine corrector were kept at the same height, different field of view in another word, differences among diurnal patterns of ITs of the four systems showed the same features as those shown in Figure A5, when the bare fiber and cosine corrector were set at different heights. The IT of SII was always the shortest and was generally shorter than 1 second, proving that using prism to switch between the downwelling and upwelling optic paths could reducing photons loss compared to using splitter fiber add TTL to switch between the two paths.

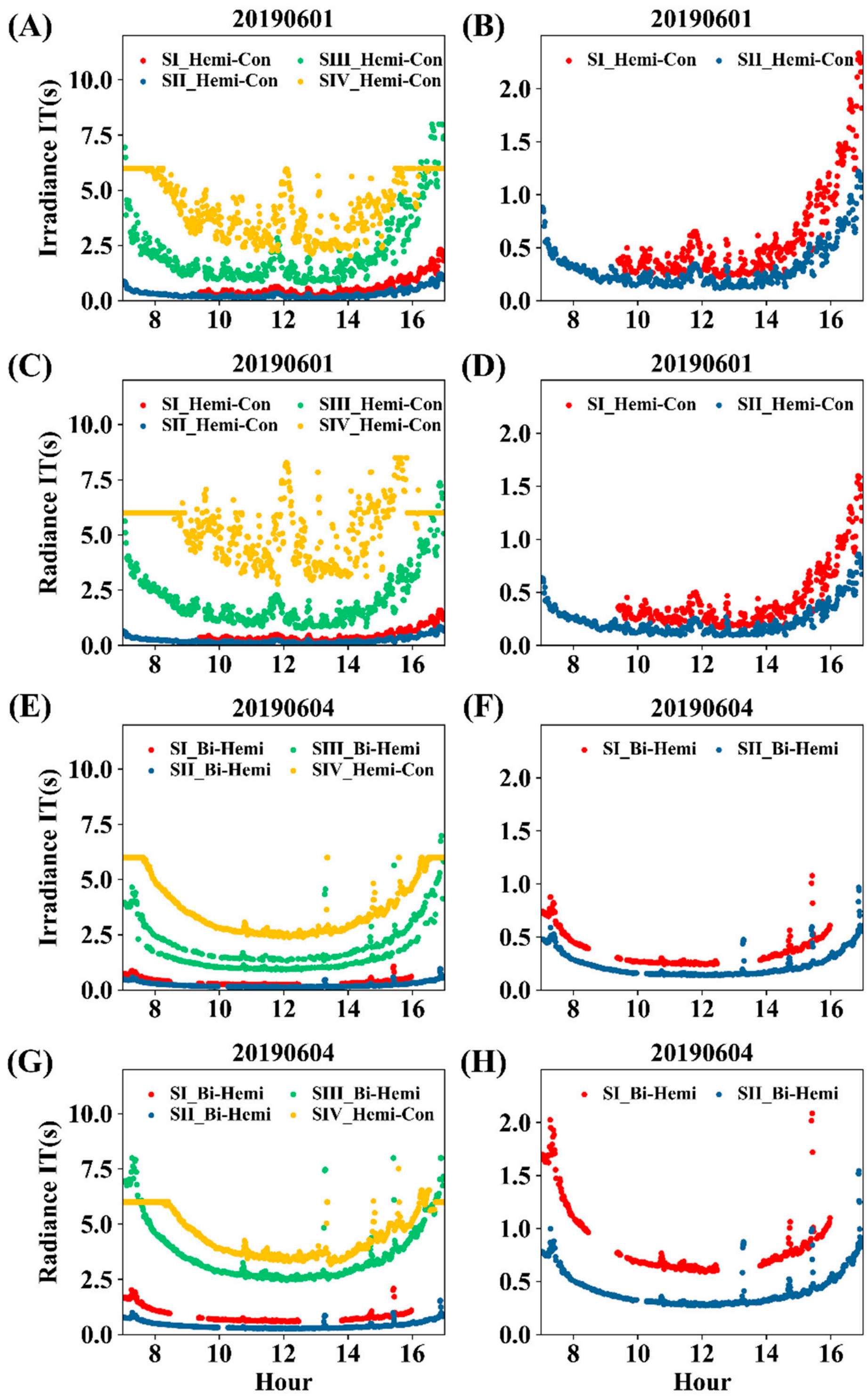

Figure A5. Diurnal variations of integration time of different systems of (A-D) hemi-con and (E-H) Bi-Hemi configurations while the upwelling sensors pointing toward vegetation at the same viewer height (different field of view). The right volume specifically shows integration times of SI and SII.

References

1. Huete, A.; Didan, K.; Miura, T.; Rodriguez, E.P.; Gao, X.; Ferreira, L.G. Overview of the radiometric and biophysical performance of the modis vegetation indices. *Remote Sens. Environ.* **2002**, *83*, 195–213. [CrossRef]
2. Dobrowski, S.; Pushnik, J.; Zarco-Tejada, P.J.; Ustin, S.L. Simple reflectance indices track heat and water stress-induced changes in steady-state chlorophyll fluorescence at the canopy scale. *Remote Sens. Environ.* **2005**, *97*, 403–414. [CrossRef]
3. Frankenberg, C.; Berry, J.; Guanter, L.; Joiner, J. Remote sensing of terrestrial chlorophyll fluorescence from space. *SPIE Newsroom* **2013**. [CrossRef]
4. Frankenberg, C.; Fisher, J.B.; Worden, J.; Badgley, G.; Saatchi, S.S.; Lee, J.E.; Toon, G.C.; Butz, A.; Jung, M.; Kuze, A. New global observations of the terrestrial carbon cycle from gosat: Patterns of plant fluorescence with gross primary productivity. *Geophys. Res. Lett.* **2011**, *38*. [CrossRef]
5. Frankenberg, C.; Pollock, R.; Lee, R.; Rosenberg, R.; Blavier, J.; Crisp, D.; O'Dell, C.; Osterman, G.; Roehl, C.; Wennberg, P. The orbiting carbon observatory (oco-2): Spectrometer performance evaluation using pre-launch direct sun measurements. *Atmos. Meas. Tech.* **2015**, *8*, 301–313. [CrossRef]
6. Guanter, L.; Aben, I.; Tol, P.; Krijger, J.; Hollstein, A.; Köhler, P.; Damm, A.; Joiner, J.; Frankenberg, C.; Landgraf, J. Potential of the tropospheric monitoring instrument (tropomi) onboard the sentinel-5 precursor for the monitoring of terrestrial chlorophyll fluorescence. *Atmos. Meas. Tech.* **2015**, *8*, 1337–1352. [CrossRef]
7. Guanter, L.; Alonso, L.; Gómez-Chova, L.; Amorós-López, J.; Vila, J.; Moreno, J. Estimation of solar-induced vegetation fluorescence from space measurements. *Geophys. Res. Lett.* **2007**, *34*. [CrossRef]
8. Guanter, L.; Frankenberg, C.; Dudhia, A.; Lewis, P.E.; Gómez-Dans, J.; Kuze, A.; Suto, H.; Grainger, R.G. Retrieval and global assessment of terrestrial chlorophyll fluorescence from gosat space measurements. *Remote Sens. Environ.* **2012**, *121*, 236–251. [CrossRef]
9. Guanter, L.; Zhang, Y.; Jung, M.; Joiner, J.; Voigt, M.; Berry, J.A.; Frankenberg, C.; Huete, A.R.; Zarco-Tejada, P.; Lee, J.-E. Global and time-resolved monitoring of crop photosynthesis with chlorophyll fluorescence. *Proc. Natl. Acad. Sci. USA* **2014**, *111*, E1327–E1333. [CrossRef]
10. Sun, Y.; Frankenberg, C.; Wood, J.D.; Schimel, D.S.; Jung, M.; Guanter, L.; Drewry, D.; Verma, M.; Porcar-Castell, A.; Griffis, T.J. Oco-2 advances photosynthesis observation from space via solar-induced chlorophyll fluorescence. *Science* **2017**, *358*, eaam5747. [CrossRef]
11. Walther, S.; Voigt, M.; Thum, T.; Gonsamo, A.; Zhang, Y.; Köhler, P.; Jung, M.; Varlagin, A.; Guanter, L. Satellite chlorophyll fluorescence measurements reveal large-scale decoupling of photosynthesis and greenness dynamics in boreal evergreen forests. *Glob. Chang. Biol.* **2016**, *22*, 2979–2996. [CrossRef] [PubMed]
12. Cogliati, S.; Rossini, M.; Julitta, T.; Meroni, M.; Schickling, A.; Burkart, A.; Pinto, F.; Rascher, U.; Colombo, R. Continuous and long-term measurements of reflectance and sun-induced chlorophyll fluorescence by using novel automated field spectroscopy systems. *Remote Sens. Environ.* **2015**, *164*, 270–281. [CrossRef]
13. Grossmann, K.; Frankenberg, C.; Magney, T.S.; Hurlock, S.C.; Seibt, U.; Stutz, J. Photospec: A new instrument to measure spatially distributed red and far-red solar-induced chlorophyll fluorescence. *Remote Sens. Environ.* **2018**, *216*, 311–327. [CrossRef]
14. MacArthur, A.; Robinson, I.; Rossini, M.; Davis, N.; MacDonald, K. A dual-field-of-view spectrometer system for reflectance and fluorescence measurements (piccolo doppio) and correction of etaloning. In Proceedings of the Fifth International Workshop on Remote Sensing of Vegetation Fluorescence, Paris, France, 22–24 April 2014; pp. 22–24.
15. Pinto, F.; Damm, A.; Schickling, A.; Panigada, C.; Cogliati, S.; Muller-Linow, M.; Balvora, A.; Rascher, U. Sun-induced chlorophyll fluorescence from high-resolution imaging spectroscopy data to quantify spatio-temporal patterns of photosynthetic function in crop canopies. *Plant Cell Environ.* **2016**, *39*, 1500–1512. [CrossRef] [PubMed]
16. Pinto, F.; Müller-Linow, M.; Schickling, A.; Cendrero-Mateo, M.; Ballvora, A.; Rascher, U. Multiangular observation of canopy sun-induced chlorophyll fluorescence by combining imaging spectroscopy and stereoscopy. *Remote Sens.* **2017**, *9*, 415. [CrossRef]
17. Porcar Castell, A.; Mac Arthur, A.; Rossini, M.; Eklundh, L.; Pacheco Labrador, J.; Anderson, K.; Balzarolo, M.; Martín, M.; Jin, H.; Tomelleri, E. Eurospec: At the interface between remote sensing and ecosystem CO_2 flux measurements in europe. *Biogeosciences* **2015**, *12*, 6103–6124. [CrossRef]

18. Yang, X.; Tang, J.; Mustard, J.F.; Lee, J.E.; Rossini, M.; Joiner, J.; Munger, J.W.; Kornfeld, A.; Richardson, A.D. Solar-induced chlorophyll fluorescence that correlates with canopy photosynthesis on diurnal and seasonal scales in a temperate deciduous forest. *Geophys. Res. Lett.* **2015**, *42*, 2977–2987. [CrossRef]
19. Zhang, Q.; Fan, Y.; Zhang, Y.; Chou, S.; Ju, W.; Chen, J.M. A conjunct near-surface spectroscopy system for fix-angle and multi-angle continuous measurements of canopy reflectance and sun-induced chlorophyll fluorescence. In *Remote Sensing System Engineering VI*; International Society for Optics and Photonics: Bellingham, WA, USA, 2016; p. 99770C.
20. Balzarolo, M.; Anderson, K.; Nichol, C.; Rossini, M.; Vescovo, L.; Arriga, N.; Wohlfahrt, G.; Calvet, J.-C.; Carrara, A.; Cerasoli, S. Ground-based optical measurements at european flux sites: A review of methods, instruments and current controversies. *Sensors* **2011**, *11*, 7954–7981. [CrossRef]
21. Daumard, F.; Champagne, S.; Fournier, A.; Goulas, Y.; Ounis, A.; Hanocq, J.-F.; Moya, I. A field platform for continuous measurement of canopy fluorescence. *IEEE Trans. Geosci. Remote Sens.* **2010**, *48*, 3358–3368. [CrossRef]
22. Burkart, A.; Schickling, A.; Mateo, M.P.C.; Wrobel, T.J.; Rossini, M.; Cogliati, S.; Julitta, T.; Rascher, U. A method for uncertainty assessment of passive sun-induced chlorophyll fluorescence retrieval using an infrared reference light. *IEEE Sens. J.* **2015**, *15*, 4603–4611. [CrossRef]
23. Du, S.; Liu, L.; Liu, X.; Guo, J.; Hu, J.; Wang, S.; Zhang, Y. Sifspec: Measuring solar-induced chlorophyll fluorescence observations for remote sensing of photosynthesis. *Sensors* **2019**, *19*, 3009. [CrossRef] [PubMed]
24. Miao, G.; Guan, K.; Yang, X.; Bernacchi, C.J.; Berry, J.A.; DeLucia, E.H.; Wu, J.; Moore, C.E.; Meacham, K.; Cai, Y. Sun-induced chlorophyll fluorescence, photosynthesis, and light use efficiency of a soybean field from seasonally continuous measurements. *J. Geophys. Res. Biogeosci.* **2018**, *123*, 610–623. [CrossRef]
25. Rossini, M.; Nedbal, L.; Guanter, L.; Ač, A.; Alonso, L.; Burkart, A.; Cogliati, S.; Colombo, R.; Damm, A.; Drusch, M. Red and far red sun-induced chlorophyll fluorescence as a measure of plant photosynthesis. *Geophys. Res. Lett.* **2015**, *42*, 1632–1639. [CrossRef]
26. Zhang, Y.; Xiao, X.; Zhang, Y.; Wolf, S.; Zhou, S.; Joiner, J.; Guanter, L.; Verma, M.; Sun, Y.; Yang, X. On the relationship between sub-daily instantaneous and daily total gross primary production: Implications for interpreting satellite-based sif retrievals. *Remote Sens. Environ.* **2018**, *205*, 276–289. [CrossRef]
27. Yang, X.; Shi, H.; Stovall, A.; Guan, K.; Miao, G.; Zhang, Y.; Zhang, Y.; Xiao, X.; Ryu, Y.; Lee, J.-E. Fluospec 2—An automated field spectroscopy system to monitor canopy solar-induced fluorescence. *Sensors* **2018**, *18*, 2063. [CrossRef]
28. Meroni, M.; Barducci, A.; Cogliati, S.; Castagnoli, F.; Rossini, M.; Busetto, L.; Migliavacca, M.; Cremonese, E.; Galvagno, M.; Colombo, R. The hyperspectral irradiometer, a new instrument for long-term and unattended field spectroscopy measurements. *Rev. Sci. Instrum.* **2011**, *82*, 043106. [CrossRef]
29. Pacheco-Labrador, J.; Hueni, A.; Mihai, L.; Sakowska, K.; Julitta, T.; Kuusk, J.; Sporea, D.; Alonso, L.; Burkart, A.; Cendrero-Mateo, M.P. Sun-induced chlorophyll fluorescence i: Instrumental considerations for proximal spectroradiometers. *Remote Sens.* **2019**, *11*, 960. [CrossRef]
30. Garzonio, R.; Di Mauro, B.; Colombo, R.; Cogliati, S. Surface reflectance and sun-induced fluorescence spectroscopy measurements using a small hyperspectral UAS. *Remote Sens.* **2017**, *9*, 472. [CrossRef]
31. Anderson, K.; Milton, E.; Rollin, E. Calibration of dual-beam spectroradiometric data. *Int. J. Remote Sens.* **2006**, *27*, 975–986. [CrossRef]
32. Mihai, L.; Mac Arthur, A.; Hueni, A.; Robinson, I.; Sporea, D. Optimized spectrometers characterization procedure for near ground support of esa flex observations: Part 1 spectral calibration and characterisation. *Remote Sens.* **2018**, *10*, 289. [CrossRef]
33. Sabater, N.; Middleton, E.M.; Malenovsky, Z.; Alonso, L.; Verrelst, J.; Huemmrich, K.F.; Campbell, P.K.; Kustas, W.P.; Vicent, J.; Van Wittenberghe, S. Oxygen transmittance correction for solar-induced chlorophyll fluorescence measured on proximal sensing: Application to the nasa-gsfc fusion tower. In Proceedings of the 2017 IEEE International Geoscience and Remote Sensing Symposium (IGARSS), Fort Worth, TX, USA, 23–28 July 2017; pp. 5826–5829.
34. Gu, L.; Wood, J.; Chang, C.Y.; Sun, Y.; Riggs, J. Advancing terrestrial ecosystem science with a novel automated measurement system for sun-induced chlorophyll fluorescence for integration with eddy covariance flux networks. *J. Geophys. Res. Biogeosci.* **2019**, *124*, 127–146. [CrossRef]

35. Aasen, H.; Van Wittenberghe, S.; Medina, N.S.; Damm, A.; Goulas, Y.; Wieneke, S.; Hueni, A.; Malenovský, Z.; Alonso, L.; Pacheco-Labrador, J. Sun-induced chlorophyll fluorescence II: Review of passive measurement setups, protocols, and their application at the leaf to canopy level. *Remote Sens.* **2019**, *11*, 927. [CrossRef]
36. Julitta, T. Optical Proximal Sensing for Vegetation Monitoring. Ph.D. Thesis, University of Milano-Bicocca, Milan, Italy, 2015.
37. Meroni, M.; Rossini, M.; Guanter, L.; Alonso, L.; Rascher, U.; Colombo, R.; Moreno, J. Remote sensing of solar-induced chlorophyll fluorescence: Review of methods and applications. *Remote Sens. Environ.* **2009**, *113*, 2037–2051. [CrossRef]
38. He, L.; Chen, J.M.; Liu, J.; Mo, G.; Joiner, J. Angular normalization of gome-2 sun-induced chlorophyll fluorescence observation as a better proxy of vegetation productivity. *Geophys. Res. Lett.* **2017**, *44*, 5691–5699. [CrossRef]
39. Liu, L.; Liu, X.; Wang, Z.; Zhang, B. Measurement and analysis of bidirectional sif emissions in wheat canopies. *IEEE Trans. Geosci. Remote Sens.* **2015**, *54*, 2640–2651. [CrossRef]
40. Zhang, Z.; Zhang, Y.; Joiner, J.; Migliavacca, M. Angle matters: Bidirectional effects impact the slope of relationship between gross primary productivity and sun-induced chlorophyll fluorescence from orbiting carbon observatory-2 across biomes. *Glob. Chang. Biol.* **2018**, *24*, 5017–5020. [CrossRef]
41. Zhang, Y.; Wang, S.; Liu, L.; Ju, W.; Zhu, X. Chinaspec: A network of sif observations to bridge flux measurements and remote sensing data. In Proceedings of the Agu Fall Meeting, New Orleans, LA, USA, 11–15 December 2017.
42. Zarco-Tejada, P.J.; González-Dugo, V.; Williams, L.; Suárez, L.; Berni, J.A.; Goldhamer, D.; Fereres, E. A pri-based water stress index combining structural and chlorophyll effects: Assessment using diurnal narrow-band airborne imagery and the cwsi thermal index. *Remote Sens. Environ.* **2013**, *138*, 38–50. [CrossRef]
43. Liu, X.; Liu, L.; Hu, J.; Du, S. Modeling the footprint and equivalent radiance transfer path length for tower-based hemispherical observations of chlorophyll fluorescence. *Sensors* **2017**, *17*, 1131. [CrossRef]
44. Plascyk, J.A.; Gabriel, F.C. The fraunhofer line discriminator mkii-an airborne instrument for precise and standardized ecological luminescence measurement. *IEEE Trans. Instrum. Meas.* **1975**, *24*, 306–313. [CrossRef]
45. Plascyk, J.A. The mk ii fraunhofer line discriminator (fld-ii) for airborne and orbital remote sensing of solar-stimulated luminescence. *Opt. Eng.* **1975**, *14*, 144339. [CrossRef]
46. Theisen, A.F. Detecting chlorophyll fluorescence from orbit: The fraunhofer line depth model. In *From Laboratory Spectroscopy to Remotely Sensed Spectra of Terrestrial Ecosystems*; Springer: Berlin, Germany, 2002; pp. 203–232.
47. Meroni, M.; Colombo, R. Leaf level detection of solar induced chlorophyll fluorescence by means of a subnanometer resolution spectroradiometer. *Remote Sens. Environ.* **2006**, *103*, 438–448. [CrossRef]
48. Maier, S.W.; Günther, K.P.; Stellmes, M. Sun-induced fluorescence: A new tool for precision farming. In *Digital Imaging and Spectral Techniques: Applications to Precision Agriculture and Crop Physiology*; American Society of Agronomy: Madison, WI, USA, 2003; pp. 209–222. [CrossRef]
49. Schaepman, M.E.; Dangel, S. Solid laboratory calibration of a nonimaging spectroradiometer. *Appl. Opt.* **2000**, *39*, 3754–3764. [CrossRef] [PubMed]